CHAPTER IV

TURBULENCE MEASUREMENTS BY THE CROSSED-BEAM TECHNIQUE

by

M. Y. Su
Northrop - Huntsville, Alabama

and

F. R. Krause
NASA - Marshall Space Flight Center

SUMMARY

An analytical relationship which approximates the probability density of wind component variations through the cross-correlation of the passive photometer outputs of the cross-beam detection system is presented. Specifically, the probability density is shown to be proportional to the cross-correlation of the first time derivatives of the time histories of fluctuating radiation intensities which are monitored by two non-parallel photodetectors. The direction of the measured wind component is normal to both lines-of-sight of the photodetectors. Special data conditioning and handling methods for evaluating the cross-correlation of the signal time derivatives are described, and their effects on the cross-correlation and corresponding spectral densities are discussed. The new analytical relationship and data handling techniques were applied to actual atmospheric crossed-beam field test data. The reduced optically and remotely detected probability density of wind component variations was found to be in reasonable agreement with that obtained by the conventional anemometer readings. Turbulent intensity can be easily evaluated once the probability density is measured. The optical technique can also be applied to other high-temperature, chemically reactive or supersonic turbulent flows such as rocket exhausts, jet plumes, and plasma in nuclear engines. The flow fields associated with these problems still defy accurate measurements by other presently available instrumentation.

NOMENCLATURE

Symbol	Definition
B	bandwidth
$D(\xi)$	factor representing the degree of decay with respect to ξ
$E(\xi)$	function defined by equation (29)
f	frequency
f_c	cutoff frequency in a low-pass filter
f_ℓ	lower frequency in a time history
f_T	terminate frequency in a low-pass filter
f_u	upper frequency in a time history
$G_{AB}(\xi,f)$	gain of $S_{AB}(\xi,f)$
$G_{AB}^{(2)}(\xi,f)$	gain of $S_{AB}^{(2)}(\xi,f)$
$H(f)$	frequency complex frequency response
$h(\tau)$	filter transfer function
$\tilde{H}_\ell(f)$	frequency response of the Martin-Graham type roll-off low-pass filter
$\tilde{h}_\ell(t)$	transfer function of the Martin-Graham type roll-off low-pass filter
$i_A(t)$	fluctuating component of photometer A's output
$i_B(t)$	fluctuating component of photometer B's output
L_τ	integral time scale of atmospheric turbulence
N	total number of digital samples
N_m	total number of digital samples in m^{th} class

Symbol	Definition
$P(\xi, \tau_m)$	probability density of transit times in mth class
$P(U)$	probability density of wind component U
$R_{AB}(\tau)$	cross-correlation of i_A and i_B
$R_m(\xi, \tau_\ell)$	cross-correlation of samples from mth class
$R_{AB}^{(2)}(\xi, \tau_\ell)$	cross-correlation of $\partial i_A/\partial t$ and $\partial i_B/\partial t$
$S_{AB}(\xi, f)$	spectral density of $R_{AB}(\xi, \tau)$
$S_{AB}^{(2)}(\xi, f)$	spectral density of $R_{AB}^{(2)}(\xi, \tau)$
T	total length of photometer output
$\triangle T$	length of each piece of photometer output
t	time
$\triangle t$	sampling interval of digital time history
U	wind component normal to both light beams
$\bar{U}$	mean wind component
U_m	wind component associated with mth class
$\triangle U$	resolution in the wind component U
V	wind speed
X(f)	Fourier transfer of x(t)
x_{m_k}	kth sample of mth class of x(t)
x(t)	common signal in $i_A(t)$
Y(f)	Fourier transform of y(t)
y_{m_ℓ}	ℓth sample of mth class of y(t)
y(t)	common signal in $i_B(t)$

Symbol	Definition
Greek Letters	
$\epsilon(f,N_d)$	measure of error in the frequency response for using N_d samples
θ	angle between the wind vector and the normal to both light beams
ξ	normal separation distance between two beams
ξ^*	normal separation distance between A and the imaginary beam B^*
σ_u	root mean square of the wind component U
τ	time lag between i_A and i_B
Operators	
$\overline{( )}_i$	$\frac{1}{\Delta T}\int_{(i-1)\Delta T}^{i\Delta T} ( )\, dt$ piecewise average of ( )
$\overline{\overline{( )}}_m$	accumulative average over m piecewise averages
$\overline{\overline{( )}}_m$	$\left\{\frac{1}{m(m-1)}\sum_{i=1}^{m}[\overline{( )}_i - \overline{\overline{( )}}_m]^2\right\}^{1/2}$ confidence level of accumulation average
$\overline{\overline{\delta R_m}}$	$\frac{1}{\bar{\bar{\sigma}}_{xm}\,\bar{\bar{\sigma}}_{ym}}\left\{\frac{1}{2\tau_m}\int_{-Jm}^{+Jm}\Delta^2\,\bar{\bar{R}}_m(j)\,dJ\right\}^{1/2}$ relative statistical error of correlation or covariance functions.

IV-1. INTRODUCTION

Remote optical detection techniques are being developed by the Marshall Space Flight Center to provide a means for continuous monitoring of atmospheric wind and turbulence. Successful detection of most probable wind speed at an altitude of about 100 meters by these techniques has been reported [IV-1, -2].

The capability of these techniques has been extended to atmospheric turbulence measurements by optically retrieving the probability density of wind component variations. Direction of the wind component is normal to both lines-of-sight of the photometers employed. The mean, rms, and other higher moments of wind component variations may be easily evaluated from the probability density. Preliminary results on this progress with emphasis on the signal/noise analysis and electro-optical system were reported in reference IV-3.

The optical technique essentially consists of two photodetectors to monitor the optical fluctuations of natural scattered radiations which result from both spatial and temporal variations of atmospheric inhomogeneities. Each photodetector output will thus contain the information of the atmospheric inhomogeneities along its entire field of view. The cross-correlation of these two photometer outputs should reveal the characteristics of the local optical disturbance and atmospheric motion which are common to both fields of view of the two photodetectors. To have an optimum spatial resolution the two lines-of-sight of detectors should be so oriented that they are normal (but separated) to each other. This is the reason for calling this optical technique the crossed-beam technique. Because of the very low signal-to-noise ratio associated with the remotely detected radiation fluctuations, special data conditioning and processing and statistical analyses are needed for evaluating the cross-correlation of the photometer outputs and their time derivatives.

This paper presents the theoretical basis for optical approximations of turbulence levels, together with the necessary additional considerations on data conditioning and processing. In section IV-2, a theoretical relationship between the cross-correlation of the first-time derivatives of the photometer outputs and the probability density of the wind component variations is derived. This wind component is normal to both lines-of-sight of the photometers. Use of the time derivative of the photometer outputs instead of the outputs themselves is one of the essential features which differ from the previous crossed-beam detection of the most probable wind component.

Section IV-3 describes the special data conditioning and processing, and discusses their effect on the cross-correlations and corresponding spectral densities. These considerations are very important for dealing with cross-correlating time derivatives of random time histories.

Section IV-4 presents some experimental and computed results from applying the theoretical relationship and data handling methods to atmospheric crossed-beam field test data. The optically detected probability densities of the wind component variations were then compared with those independently measured by the conventional anemometers mounted on a close-by meteorological tower. The minimum separation of the crossed-beam arrangement was set directly upstream of the anemometer about 60 meters above the ground.

The authors wish to thank the following persons for their contributions to this paper: Professor V. Sandborn, Colorado State University, for carrying out the atmospheric crossed-beam field tests; Messrs. J. Jones and R. Graham, Computation Laboratory, MSFC, for digitization of test tapes, cross-correlation computation and the program for digital filtering; Mr. J. Pooley, Northrop Corporation, for programming an updated version of the error accumulation and spectral decomposition subroutines; and Dr. W. H. Heybey, MSFC, and Dr. L. N. Wilson, IITRI, for their very helpful and constructive critical reviews and comments on the extension of the crossed-beam concept to turbulence measurements.

IV-2. PROBABILITY DENSITY OF WIND COMPONENT VARIATIONS FROM OPTICAL CORRELATION

Wind speeds and directions vary, in general, fairly rapidly. To specify completely the statistics of such wind characteristics, either an infinite series of correlation functions of all orders of wind fluctuations, or an infinite series of all orders of probability densities of wind fluctuations will be needed. However, in usual meteorological applications, only limited quantities are measured, i.e., the first few moments of the wind fluctuations such as the mean wind speed, and the rms wind speed fluctuations.

When the wind direction is constant but unknown, and the speed is varying, it has been shown [IV-4, -5] that both the wind direction and speed can be simultaneously measured by the crossed-beam system. When the wind direction varies, only the wind component normal to the two lines-of-sight of detectors can be measured. The reason is that the crossed-beam measurement gives the transit time of the optical disturbance between two beams only, while the location of the transit path and its length between two beams cannot be determined unless the wind direction remains constant over the period of measurement (see Figure IV.1). Fortunately, the fixed position of two light beams gives a uniquely determined minimum separation between two beams which is in the direction normal to both beams. Thus, the combination of the measured transit time and the shortest beam separation always determine uniquely the wind component normal to both beams. Since, in most meteorological conditions,

the wind direction does vary in the minimum required period of crossed-beam measurements, we shall deal with this wind component throughout this paper.

The first-order probability density of the wind component can be measured by the crossed-beam system to a high degree of approximation. This approximation results from some relatively weak assumptions introduced in order to establish an explicit analytical relationship between the cross-correlation of optical fluctuations and the probability of wind component variations. Also, because of the variation of the wind direction, the resolution of the altitude of the prevailing wind will be questionable from one pair of crossed beams. However, if more than two pairs of crossed beams are used, which are so oriented that mutually perpendicular wind components are to be measured, then the wind direction can be approximately determined also.

The basic geometrical arrangement of the crossed-beam system is shown in Figure IV.1. The various fields of view of two ground-based photometers, A and B, are oriented so that their lines-of-sight differ by 180 degrees in the azimuth angles. Such an orientation will give the wind component both horizontal to the ground and normal to both beams. The wind component will be the one used for this discussion, unless otherwise specified.

Atmospheric inhomogeneities, such as the variations in density of aerosol, various gases and water vapor, will cause both spatial and temporal variations in radiation processes. These radiations include light scattering, absorption, and emission. Thus, the characteristics of local light fluctuations should reflect the characteristics of the atmospheric inhomogeneity (or turbulence). The atmospheric inhomogeneities are transported according to the general rules of fluid dynamics. The lifetime of the atmospheric inhomogeneity, which is a measure of the average time lapse for the inhomogeneity to retain its character (or signature), is finite; so is the lifetime of the optical fluctuation, if the light source can be considered to be relatively constant. The optical detectors A and B thus record the time histories of accumulative radiation outputs within their entire field of view, respectively. Fluctuations of the photometer output, $i_A(t)$ and $i_B(t)$, therefore contain information on the atmospheric motions along the entire line-of-sight. The mean value of the photometer outputs is not of concern here. The fluctuating part is separated from the total recording signal by A.C.-coupling electronic circuitry.

When the two beams actually intersect each other at a certain height (Figure IV.2), the local optical fluctuations radiating from the intersection region will result in some common signals in the outputs of the detectors. The common signals may not be exactly the same, but they are

related, so that the photometer outputs may be expressed as

$$\begin{aligned} i_A(t) &= x(t) + i_{A,n}(t) \\ i_B(t) &= y(t) + i_{B,n}(t). \end{aligned} \tag{1}$$

Here, $x(t)$ and $y(t)$ are the common signals mentioned above, while $i_{A,n}(t)$ and $i_{B,n}(t)$ are light fluctuations outside the intersection region. In contrast to desired common signals, they will be called noises due to transmission, or flow noises. By the nature of the atmospheric inhomogeneities, all the terms in equation (1) are random time histories. The most powerful method available to retrieve such common signals is the correlation technique, which is commonly used in the communication theory and random vibration analysis. A correlation function is computed by adding the products of two time histories, i_A and i_B. That is,

$$R_{AB}(\tau) = \langle i_A(t) i_B(t+\tau) \rangle \equiv \lim_{T\to\infty} \frac{1}{T} \int_o^T i_A(t)\ i_B(t+\tau)\ dt. \tag{2}$$

Substituting equation (1) into (2) yields

$$\begin{aligned} R_{AB}(\tau) = &\langle x(t)y(t+\tau) \rangle + \langle x(t)\ i_{B,n}(t+\tau) \rangle + \langle i_{A,n}(t) y(t+\tau) \rangle \\ &+ \langle i_{A,n}(t)\ i_{B,n}(t+\tau) \rangle . \end{aligned} \tag{3}$$

The first term in the right-hand side of the above equation is the cross-correlation between two common signals. The other three terms are the cross-correlation among statistically unrelated light fluctuations; thus, they will vanish if the integration time T is long enough. That is, the time integration will suppress "noise" components. In actual application, the integration time T is always finite. The uncertainty (or error) due to this finite T will be discussed further in section V. For a sufficiently long integration time, which is also the length of the time histories, equation (3) can be written approximately as

$$R_{AB}(\tau) \cong \langle x(t)y(t+\tau) \rangle. \tag{4}$$

This means that as long as one deals with such product mean values, one can disregard all light modulations that are not common to both fields of view of the two detectors [IV-6].

To measure the wind component the two beams have to be separated. The shortest separation distance is denoted by ξ. The common signals in the two detectors now are caused by the convected atmospheric inhomogeneities which happen to traverse both light beams. The time lapse which an inhomogeneity takes to travel from one beam, say A, to the other beam, B, will be called the "transit time." The distance between the two beams of the traversing path $\overline{CD}$ will be called the "transit distance." Associated with the transit path is the transit height, which is the altitude of the transit path above the ground (see Figure IV.1). When the wind speed, V, and direction, θ, are fixed, the associated transit time can be obtained from the cross-correlation curve (equation (4)). It is the time lag associated with the maximum value (or peak) of $R_{AB}(\tau)$, denoted by τ_{peak}. On the other hand, the transit distance cannot be determined unless the wind direction is known. Without knowing the wind direction, the best one can deduce is the component of the transit distance in the direction normal to both light beams, which is simply the shortest distance ξ. Thus, the relationship between the wind component U and the time lag τ_{peak} from the crossed-beam measurement is

$$U = V \cos \theta = \frac{\overline{CD}}{\tau_{peak}} \cos \theta = \frac{\xi/\cos \theta}{\tau_{peak}} \cos \theta$$

or

$$U = \frac{\xi}{\tau_{peak}} . \qquad (5)$$

Here, the distance ξ is fixed by the crossed-beam arrangement, which is completely known. Hence, equation (5) allows us to measure the wind component through the remote detection of the optical fluctuations and the cross-correlation of these fluctuations if the wind speed and direction remain constant.

The more realistic meteorological situations are those where the wind speed and direction both change with time. Under such situations, the maximum information that can be retrieved from the cross-correlation of the optical fluctuations is the first-order probability density of the wind component variations.

We shall now derive the relationship of the cross-correlation of crossed-beam signals to the probability density of the wind component variations. As discussed above, all the noise components in the two photometer outputs $i_A(t)$ and $i_B(t)$ will be suppressed through cross-correlation. We need only to consider the two time histories of common (desired) signals, x(t) and y(t), without loss of generality. Let the time histories of length T be digitized with a sampling interval, Δt. The total number of digital samples for either time history will be denoted by N:

$$N = \frac{T}{\Delta t} .$$

These digital samples and digital time lags will be denoted as follows:

$$\begin{aligned} x_n &= x(t = n\,\Delta t) \\ y_n &= y(t = n\,\Delta t) \end{aligned} \qquad (6)$$

and

$$\tau_\ell = \ell\,\Delta t,$$

where $n = 1,2, \ldots, N$ and $\ell = 0,1,2, \ldots, L \ll N$.

Since the wind component may vary over the period of measurement, T, the associated transit time may also vary correspondingly. Without loss of generality, we shall assume that the beam A lies in the upstream of beam B. Each digital sample x_n will then have a corresponding digital sample $y_{n+\ell}$. They are attributed to the same atmospheric inhomogeneity which takes the time lag $\tau_\ell = \ell\,\Delta t$ to travel from some point in beam A to another point in beam B. The transit path between these two points is not necessarily straight. It can be of any shape. The corresponding wind component normal to both beams is ξ/τ_ℓ. The cross-correlation (equation (4)) can now be written in the summation form as

$$R_{AB}(\tau_\ell) = \frac{1}{N} \sum_{n=1}^{N} x_n\, y_{n+\ell}. \qquad (7)$$

It should be noted that the value of the summation is invariant under any different ways of grouping the terms $x_n y_{n+\ell}$ in the summation. For

the purpose of retrieving variations of the wind component, the digital samples x_n may be classified with respect to their associated transit times. Let the class interval for transit times be the same as the sampling interval Δt. The mth class of transit times, denoted by τ_m, will be defined as

$$\tau_m: \quad m\,\Delta t \leq \tau_m < (m+1)\,\Delta t, \tag{8}$$

where m = 0,1,2, ..., M. M is any integer that is large enouth to cover all possible transit times of interest. The corresponding mth class of wind components denoted by U_m will be

$$U_m: \quad \frac{\xi}{(m+1)\,\Delta t} < U_m \leq \frac{\xi}{m\,\Delta t}\ . \tag{9}$$

Now group those digital samples x_n according to the classification of equation (8). Further, denote the kth sample in the mth class in the ascending order of time by

$$x_{m_k} = x(t = m_k\,\Delta t) \tag{10}$$

and the total number of digital samples belonging to this class by N_m. Thus,

$$N = \sum_{m=0}^{M} N_m. \tag{11}$$

The probability density of transit times of the mth class over the period T of measurement can be expressed as

$$P(\xi, \tau_m)\,\Delta t \equiv P[\xi,\ m\,\Delta t \leq \tau_m < (m+1)\,\Delta t]\,\Delta t = \frac{N_m}{N}\ . \tag{12}$$

The corresponding probability density of the wind components $P(U_m)$ can be obtained from the above probability density by a transformation of variables from the transit time to the wind component.

$$P(U_m) \equiv P\left[\frac{\xi}{(m+1)\,\Delta t} < U_m \leq \frac{\xi}{m\,\Delta t}\right]$$

$$= P(\xi, \tau_m) \left|\frac{d\tau_m}{dU_m}\right| = \frac{\tau_m^2}{\xi} P(\xi, \tau_m). \tag{13}$$

With the above classification of digital samples and definitions of the probability density, the cross-correlation of the optical fluctuations from the photometers can be expressed as

$$R_{AB}(\tau_\ell) = \frac{1}{N} \sum_{n=0}^{N} x_m \, y_{n+\ell}$$

$$= \frac{1}{N} \sum_{m=0}^{M} \sum_{k=1}^{N_m} x_{m_k} \, y_{m_k+\ell}$$

$$= \sum_{m=0}^{M} \frac{N_m}{N} \left[\frac{1}{N_m} \sum_{k=1}^{N_m} x_{m_k} \, y_{m_k+\ell}\right]. \tag{14}$$

Let us define the term in the parentheses by

$$R_m(\xi, \tau_\ell) = \frac{1}{N_m} \sum_{k=1}^{N_m} x_{m_k} \, y_{m_k+\ell}. \tag{15}$$

By substituting equations (12) and (15), equation (14) can be written as

$$R_{AB}(\xi, \tau_\ell) = \frac{1}{N_m} \sum_{m=0}^{M} P(\xi, \tau_m) \, R_m(\xi, \tau_\ell) \, \Delta\tau_m \quad (\text{with } \Delta\tau_m = \Delta t). \tag{16}$$

Clearly, the function $R_m(\xi, \tau_\ell)$ represents the cross-correlation of the mth class of digital samples. Equation (16) simply states that the total cross-correlation $R_{AB}(\xi, \tau_\ell)$ is equal to the sum of M + 1 cross-correlation of each individual class of samples with the associated probability density of transit times during measurement T as a weighting factor.

In almost all actual applications, both functions $P(\xi, \tau_m)$ and $R_m(\xi, \tau_m)$ can be assumed to be continuous with respect to τ_m; thus, the above summation can be written in the integral form as the increment $\Delta\tau_m$ becomes very small (i.e., $\Delta\tau_m \to 0$).

$$R_{AB}(\xi, \tau_\ell) = \int_0^\infty P(\xi, \tau_m)\, R_m(\xi, \tau_\ell)\, d\tau_m. \tag{17}$$

Strictly speaking, this limiting process $\Delta\tau_m \to 0$ cannot be applied, since this would require the knowledge of the infinitesimal wind component fluctuations. It is known that the highest wind fluctuation measurable by the crossed-beam technique is dictated by the beam separation distance ξ and the maximum prevailing wind component. Specifically, the highest resolution in the wind component is given by

$$\Delta U = \frac{\xi}{\tau_{max}}, \tag{18}$$

where τ_{max} is the maximum time lag used in R_{AB}. This is the lowest possible wind component which can be measured by the crossed-beam system, i.e.,

$$\min(U) = \Delta U = \frac{\xi}{\tau_{max}}. \tag{19}$$

The highest frequency fluctuation of the wind component is given by

$$\max(f_u) = \frac{U_{max}}{2\pi\xi}, \tag{20}$$

where U_{max} is the maximum possible wind component in that particular measurement under consideration. However, we applied the limiting process in the sense of numerical equivalence between equations (16) and (17), which offers a high degree of approximation. Equation (17) is an integral equation for the desired (unknown) probability density of transit times. The simplest possible way to solve for $P(\xi, \tau_m)$ is to uncouple interactions between $P(\xi, \tau_m)$ and $R_m(\xi, \tau_\ell)$ so that the probability density can be expressed in terms of the experimentally accessible cross-correlation. The desired uncoupling is feasible with suitable data conditioning on the photometer outputs under some relatively weak assumptions regarding atmospheric turbulence and wind characteristics. This will now be discussed.

We shall first make an assumption (I) that samples in each class will decay by the same amount in their turbulent characteristics over the same beam separation and that the rate of decay may differ in different classes of samples. According to Bachelor [IV-7], the decay of relative turbulent energy, which is defined as the ratio of the mean square of speed fluctuations to the square of the mean speed, is linearly proportional to the transit distance. The turbulent fluctuation in the photometer outputs is a mixed outcome of fluctuations both in the flow speed and the extinction coefficient of the flow medium. Nevertheless, the assumption would be at least the first order approximation for a transit distance of the order of several integral length scales of atmospheric inhomogeneities. The second assumption (II) is that the number of samples in each class, which is classified at the upstream beam A, is the same if the classification were made at the downstream beam B. This assumption is really a restriction which excludes the consideration of wind component fluctuations with frequency higher than max $[f_u]$ (see equation (20)). By using these two assumptions, the cross-correlation of mth class of samples (equation (18)) can be rewritten as

$$R_m(\xi, \tau_\ell) = D(\xi)\ R(\xi^* \equiv \xi - U_m \tau_\ell,\ 0) \tag{21}$$

or

$$R_m(\xi, \tau_\ell) = D(\xi)\ R(\xi^* = \xi(1 - \frac{\tau_\ell}{\tau_m}),\ 0), \tag{22}$$

where $D(\xi)$ is a factor representing decay of turbulence with respect to the separation distance, while the space-time cross-correlation $R_m(\xi, \tau_\ell)$ is replaced by an equivalent spatial cross-correlation $R(\xi^*, 0)$ with imaginary translation of the downstream beam B closer to the upstream beam A by the amount of $U_m \tau$ for compensating the convective motion of the atmospheric inhomogeneity (see Figure IV.3).

Next, substituting the approximate relationship (equation (22)) into equation (17) yields

$$R_{AB}(\xi,\tau_\ell) = D(\xi) \int_0^\infty P(\xi,\tau_m)\ R(\xi^* = \xi(1-\frac{\tau_\ell}{\tau_m}),\ 0)\ d\tau_m. \tag{23}$$

What has been accomplished in the above equation compared with the equation (17) is that the dependence of the functional form of R_m has been eliminated from the integrand. However, $P(\xi,\tau_m)$ and $R(\xi^*,0)$ is still coupled. It should be noted that the spatial cross-correlation $R(\xi^*,0)$ reaches its maximum value for $\xi^* = 0$, i.e., when the imaginary beam B^* intersects beam A. A certain correlation will persist for $0 < \xi^*$, but will be smaller than the scale of the atmospheric inhomogeneities common to both light beams. In other words, a certain correlation exists if

$$|\tau_m - \tau_\ell| = |\tau_m(1-\frac{\tau_\ell}{\tau_m})|$$

is less than the time lapse for the atmospheric inhomogeneity traversing its own length. This time lapse is usually defined by

$$L_\tau = \frac{1}{R(\xi^*=0,0)} \int_0^\infty R(\xi^*,0)\ d\tau_m, \tag{24}$$

which is normally called the integral time scale of the atmospheric inhomogeneity. For the time being, we shall introduce a third assumption (III) that the integral time scale is much smaller than the half-width of the probability density of the transit time fluctuations (see Figure IV.4). That is,

$$L_\tau << \tau_{rms} = |\tau_2 - \tau_1|, \tag{25}$$

where τ_1 and τ_2 are the two transit times such that

$$P(\xi,\tau_1) = P(\xi,\tau_2) = e^{-1/2} \max(P(\xi,\tau)). \tag{26}$$

The justification of this assumption will be discussed after equation (36). But let us examine first how this assumption will affect equation (23). This assumption essentially implies that the spatial cross-correlation $R(\xi^*)$ behaves like a Dirac delta function. The equation (23) can be approximately written as

$$R_{AB}(\xi,\tau_\ell) \cong D(\xi)\ P(\xi,\tau_\ell) \int_0^\infty R(\xi^* = \xi(1-\frac{\tau_\ell}{\tau_m}),0)\ d\tau_m. \tag{27}$$

Changing the variable in the integration from τ_m to ξ^* yields

$$R_{AB}(\xi,\tau_\ell) \cong D(\xi)\ P(\xi,\tau_\ell) \int_{-\infty}^{\infty} R(\xi^*)\ \frac{d\tau_m}{d\xi^*}\ d\xi^*$$

$$= D(\xi)\ P(\xi,\tau_\ell)\ \frac{\tau_\ell}{\xi} \int_{-\infty}^{\xi} \frac{R(\xi^*)}{(1-\frac{\xi^*}{\xi})^2}\ d\xi^*$$

$$= E(\xi)\tau_\ell\ P(\xi,\tau_\ell), \tag{28}$$

where

$$E(\xi) = \frac{D(\xi)}{\xi} \int_{-\infty}^{\infty} \frac{R(\xi^*)}{(1-\frac{\xi^*}{\xi})^2}\ d\xi^*. \tag{29}$$

Thus, the probability density of transit times can be written as

$$P(\xi,\tau_\ell) = \frac{R_{AB}(\xi,\tau_\ell)}{E(\xi)\ \tau_\ell}\ . \tag{30}$$

The dependence on the factor $E(\xi)$ can be further eliminated by normalization, since it is independent of the transit time. That is,

$$\frac{P(\xi,\tau_\ell)}{\max(P(\xi,\tau_\ell))} = \frac{R_{AB}(\xi,\tau_\ell)/\tau_\ell}{\max(R_{AB}(\xi,\tau_\ell)/\tau_\ell)} \quad . \tag{31}$$

The normalized probability density of transit times can be approximated by the measurable cross-correlation of two photometer outputs. Physically, it will be more useful to have the probability density of wind component variations. This can be accomplished by transforming the variable from the transit time τ_ℓ to the wind component U through the following relationship:

$$U = \frac{\xi}{\tau_\ell}. \tag{32}$$

The normalized probability density of wind components (normal to both light beams) P(U) can be approximated by using equation (30).

$$P(U = \frac{\xi}{\tau_\ell}) = P(\xi,\tau_\ell) \left|\frac{d\tau_\ell}{dU}\right| = \frac{\tau_\ell^2}{\xi} P(\xi,\tau_\ell)$$

$$= \frac{\tau_\ell R_{AB}(\xi,\tau_\ell)}{\xi E(\xi)} \quad . \tag{33}$$

Again, by applying the normalization procedure to the above expression, we obtain

$$\frac{P(U=\frac{\xi}{\tau_\ell})}{\max(P(U))} = \frac{R_{AB}(\xi,\tau_\ell)}{\max[\tau_\ell R_{AB}(\xi,\tau_\ell)]} \quad . \tag{34}$$

Alternatively, one may apply the characteristics of the probability density, i.e.,

$$\int_{-\infty}^{\infty} P(\xi,\tau_\ell)\, d\tau_\ell = 1, \tag{35}$$

to equation (30), and then substitute in equation (33):

$$P(U=\frac{\xi}{\tau_\ell}) = \frac{\tau_\ell \, R_{AB}(\xi,\tau_\ell)}{\xi \int_{-\infty}^{\infty} \frac{1}{\tau'_\ell} R_{AB}(\xi,\tau'_\ell) \, d\tau'_\ell} \quad . \tag{36}$$

This implies that the probability density of wind components normal to both light beams can be approximated by the measurable cross-correlation of photometer outputs. The above optical approximation is valid under the three assumptions made which are summarized as follows:

(I) Samples of common optical fluctuations in each class with the same transit time will decay by the same amount in their turbulent characteristics over the same beam separation.

(II) The number of samples in each class, which is classified at the upstream beam, is the same if the classification were made at the downstream beam.

(III) The temporal integral scale of atmospheric inhomogeneities is much shorter than the half-width of the probability density of the transit times.

The first two assumptions are fairly realistic approximations for atmospheric turbulence, provided the transit distance does not exceed about 200 meters or the transit time does not exceed about 20 seconds. On the other hand, the third assumption is usually not met in the atmosphere. The integral length scale of atmospheric inhomogeneity is between 10 to 100 meters long in the atmosphere [IV-8]. However, a shorter optical disturbance may be expected if we cross-correlate the first time derivatives $\partial x(t)/\partial t$ and $\partial y(t)/\partial t$ of the common signals $x(t)$ and $y(t)$ instead of the common signals themselves. Since we shall employ the cross-correlation technique, these two time derivatives can be simply replaced by the time derivatives of the photometer outputs $\partial i_A(t)/\partial t$ and $\partial i_B(t)/\partial t$. Physically, the integral length scale of the time derivatives is the so-called microscale of optical disturbance [IV-9]. This microscale is usually at least one order shorter than the average integral scale. Mathematically, the time derivative is the time rate of change of optical disturbance; thus, significant values of the derivative may be expected only when a large change in the optical disturbance occurs. Heuristically, if one may simply visualize an atmospheric turbulent eddy as an elongated

body with its major axis along the flow direction, then the time derivative will be directly proportional to the slope of the eddy. Therefore, only when the leading or trailing edge of the eddy passes through the light beam may a significant optical fluctuation occur. Therefore, the unrealistic assumption (III) can now be replaced by the following realistic assumption (III-A), if the time derivatives of the photometer outputs are used to evaluate the cross-correlation.

(III-A) The temporal microscale of atmospheric inhomogeneities is much smaller than the half-width of the probability density of the transit times.

With this consideration, equations (34) and (36) should then assume the following forms:

$$\frac{P(U=\frac{\xi}{\tau_\ell})}{\max(P(U=\frac{\xi}{\tau_\ell}))} = \frac{\tau_\ell \, R_{AB}^{(2)}(\xi,\tau_\ell)}{\max[\tau_\ell \, R_{AB}^{(2)}(\xi,\tau_\ell)]} \tag{37}$$

and

$$P(U=\frac{\xi}{\tau_\ell}) = \frac{\tau_\ell \, R_{AB}^{(2)}(\xi,\tau_\ell)}{\xi \int_{-\infty}^{\infty} \frac{1}{\tau'_\ell} R_{AB}^{(2)}(\xi,\tau'_\ell) \, d\tau'_\ell} \tag{38}$$

where

$$R_{AB}^{(2)}(\xi,\tau_\ell) = \frac{1}{T} \int_0^T \frac{\partial i_A(t)}{\partial t} \frac{\partial i_B(\xi,t+\tau)}{\partial t} \, dt. \tag{39}$$

For statistical stationary processes, the above expression is equivalent to the negative of the second derivative of the cross-correlation; i.e.,

$$R_{AB}^{(2)}(\xi,\tau_\ell) = -\frac{\partial^2}{\partial \tau_\ell^2} R_{AB}(\xi,\tau_\ell). \tag{40}$$

Once the probability density of the wind component variations is obtained from the cross-correlation of the time derivatives of photometer signals, all the central moments of the wind component variations can be easily calculated. The two most important moments are the mean wind component,

$$\bar{U} = \int_{-\infty}^{\infty} U\ P(U)\ dU,$$

and the mean square value (or variance) of the wind component variations,

$$\sigma_U^2 = \int_{-\infty}^{\infty} (U-\bar{U})^2\ P(U)\ dU.$$

The ratio of the root-mean-square value to the mean wind component ($\sigma_u/\bar{U}$) is a common measure of atmospheric turbulent intensity.

IV-3. DATA CONDITIONING AND PROCESSING METHODS

It was shown in the last section that the time derivatives of photometer outputs are needed for evaluating cross-correlation in order to retrieve remotely the probability density of wind component variations. For stationary atmospheric conditions, this will be equivalent to require evaluating the second derivative of the cross-correlation of the photometer outputs themselves. The atmospheric phenomena are known to be intrinsically nonstationary, but for qualitative understanding of the problems involved in the data conditioning and handling, we would assume for the moment that the time histories of photometer outputs are stationary. Under this assumption, equation (40) holds. Taking the Fourier integral transform of the equation yields

$$S_{AB}^{(2)}(\xi,f) = f^2\ S_{AB}(\xi,f), \tag{41}$$

where

$$S_{AB}^{(2)}(\xi,f) = \int_{-\infty}^{\infty} R_{AB}^{(2)}(\xi,\tau_\ell)\ e^{i2\pi f\tau_\ell} d\tau_\ell \tag{42}$$

and

$$S_{AB}(\xi,f) = \int_{-\infty}^{\infty} R_{AB}(\xi,\tau_\ell)\ e^{i2\pi f\tau_\ell}\ d\tau_\ell. \tag{43}$$

Here, $S_{AB}(\xi,f)$ is the cross-spectral density of the photometer outputs, while $S_{AB}^{(2)}(\xi,f)$ is the cross-spectral density of the first time derivatives of the photometer outputs. These two spectral densities are generally complex functions. For easier discussion, we would rather deal with their gains which are always real and defined by

$$G_{AB}^{(2)}(\xi,f) = [S_{AB}^{(2)}(\xi,f)\ S_{AB}^{(2)*}(\xi,f)]^{1/2} \tag{44}$$

and

$$G_{AB}(\xi,f) = [S_{AB}(\xi,f)\ S_{AB}^{*}(\xi,f)]^{1/2}, \tag{45}$$

where the asterisk indicates the complex conjugate. Hence, equation (41) can be rewritten as

$$G_{AB}^{(2)}(\xi,f) = f^2 G_{AB}(\xi,f). \tag{46}$$

This equation states that the gain from the time derivatives of the photometer outputs is equal to the gain from the outputs themselves multiplied by the frequency square.

In the atmosphere, the gain of the photometer outputs $G_{AB}(\xi,f)$ follows approximately f^{-2} in the range of energy-bearing eddies. This would imply that the gain from the time derivatives would approximate a white noise spectrum. It is also well known that the wider the bandwidth of a white noise spectrum, the narrower the first zero crossing of the corresponding correlation function. Thus, to better approximate the assumption (III-A), we would like to have the bandwidth of the photometer outputs as wide as possible. However, because of the following two factors, the bandwidth of the signals (i.e., the photometer outputs) should be suitably limited. First, the common signal-to-noise ratio of the photometer outputs with natural scattering radiations as light sources is very low. This ratio is usually of the order of 0.4 or less

[IV-3]. It follows that the correlation coefficient of the i_A and i_B, i.e.,

$$\frac{\langle i_A\, i_B\rangle}{\langle i_A^2\rangle^{1/2}\langle i_B^2\rangle^{1/2}}, \tag{47}$$

is of the order of $(0.4)^2 = 0.16$ or less. Such a small correlation coefficient could not be accurately evaluated by commercially available analog correlators. A digital computer is required to achieve a more complete noise cancellation by integrating over very long records without dynamic time placement errors. The f^2 weighting of the high frequency noise which is introduced by differentiating the time series also requires an additional low-pass filter with a sharp roll-off at the high frequency limit of the common signals. Secondly, in using digital computers, the time derivative may be approximated by the finite difference of two consecutive digital time samples. The quantization errors in the individual samples resulting from the analog/digital conversion will further propagate to the time derivatives [IV-11]. The main effects of the above two factors are significant only in the higher frequency portion of the cross-spectral density.

To reduce the quantization errors in the digital time histories, the sample reduction method is employed. In essence, this method consists of two steps: (1) sampling the analog time history at an interval by 2m times smaller than that required by the Nyquist's criterion, i.e., $\Delta t = 1/2(2f_u)$, where f_u is the upper frequency of the time history measured in Hertz and m is any positive integer equal or greater than 1, and (2) averaging every m consecutive digital samples to form a new digital time history with an equally spaced time interval of $1/(4f_u)$. The theory [IV-11] shows that, on the average, about 30 percent reduction in the quantization error may result by reducing five samples to one on a time history having an f^{-2} spectral density. Reductions for other spectrum shapes are also given in reference IV-11.

To determine optimum injection of f^2 weighted high frequency noise components, we have various standard frequency settings for the digital filters. Both center and roll-off frequencies were changed independently of each other. In applying the digital filtering, any desired filter gain and phase functions can easily be accomplished by using a suitable transfer function without worrying about practical limitations in electronics.

Specifically, let us consider an analog time history x(t) and let its Fourier transform be X(f), i.e.,

$$X(f) = \int_{-\infty}^{\infty} x(t)\ e^{-i2\pi ft}\ dt. \tag{48}$$

This function represents the frequency decomposition of the original time history. In a broad sense, the filter is meant to be an operator on X(f) such that X(f) will be weighted according to a desired fashion in a certain range of frequency. Mathematically, this operation can be expressed as

$$Y(f) = H(f)\ X(f). \tag{49}$$

Here, H(f) is the function characterized by the desired operation and is called the (complex) frequency response function of the filter, while Y(f) is the frequency decomposition of the output filtered random time history. The frequency response function can be broken into the real part $H_r(f)$ and imaginary part H(f), i.e.,

$$H(f) = H_r(f) + iH_i(f). \tag{50}$$

The absolute value $|H(f)|$ of H(f) is called the gain of the filter,

$$|H(f)| = [H_r^2(f) + H_i^2(f)]^{1/2}, \tag{51}$$

while the arc-tangent of the ratio $H_i(f)/H_r(f)$ is called the phase function of the filter,

$$\phi(f) = \text{arc tan } \left(\frac{H_i(f)}{H_r(f)}\right). \tag{52}$$

Denote the inverse Fourier transforms of H(f) and Y(f) to the time domain by

$$h(t) = \int_{-\infty}^{\infty} H(f) \exp(i2\pi ft)\, dt \tag{53}$$

and

$$y(t) = \int_{-\infty}^{\infty} Y(f) \exp(i2\pi ft)\, dt. \tag{54}$$

Taking the Fourier transformation of equation (49), and then substituting the above expressions, we obtain

$$y(t) = \int_{-\infty}^{\infty} h(t')\, x(t-t')\, dt'. \tag{55}$$

This equation states that the filtering as defined by equation (49) is equivalent to an integral transform of the original time history x(t) with the weighting function h(t). This weight is called the transfer function of the filter. The output of this transformation y(t) is usually called the filtered time history.

For an ideal low-pass filter with bandwidth $B = f_u$, the frequency response function is simply

$$H(f) = H(-f) = \begin{cases} 1, & |f| \leq B \\ 0, & |f| > B. \end{cases} \tag{56}$$

The corresponding transfer function will be

$$h(t) = B \frac{\sin(2\pi Bt)}{2\pi Bt}. \tag{57}$$

However, because of the Gibb's phenomenon, we cannot use the transfer function of equation (57), directly. This phenomenon essentially states

that oscillations exist in the approximating frequency response function near the discontinuities of the ideal one when one approximates an ideal frequency response function having one or more jump discontinuities with a truncated Fourier series.

To avoid this difficulty, the frequency response function is usually constructed as a continuous function. There are numerous ways to accomplish this. What we shall adopt below, one of the simplest types, is called the Martin-Graham type roll-off filter. Its frequency response function is defined for a low-pass filter [IV-12, -13] as follows:

$$\tilde{H}_{\ell}(f) = \begin{cases} 1, & |f| \leq f_c \\ \frac{1}{2}\,[1 + \cos\,\pi(f-f_c)/\Delta f], & f_c < f < f_T \\ \frac{1}{2}\,[1 + \cos\,\pi(f+f_c)/\Delta f], & f_T < f < -f_c \\ 0, & |f| \geq f_T \end{cases} \tag{58}$$

where f_c and f_T are the cutoff frequency and terminate frequency, respectively, while Δf is the frequency interval between these two frequencies, i.e., $\Delta f = f_T - f_c$. The inverse Fourier transformation of equation (58) yields the transfer function for the Martin-Graham low-pass filter:

$$\tilde{h}_{\ell}(t) = \frac{\sin(2\pi f_c t) + \sin(2\pi f_T t)}{2\pi t[1 - 4(\Delta f)^2\, t^2]} \,. \tag{59}$$

The theory for filtering and the associated equations are formulated in terms of analog time histories. To apply them to discrete digital time histories, all integrations need to be rewritten in summation forms. The frequency contents of the time history should also be known to set a suitable sampling rate for digitization following the Nyquist criterion. In actual application, the limits of integration in equation (55) will be finite.

Obviously one would like to limit the integration limits T as much as possible in order to minimize the required computer time. An explicit relation for the minimum integration time is now derived from the characteristics of both the time histories and the desired filter.

Let us denote the upper frequency in the time histories by f_u, the desired cutoff frequency of the filter by f_c, and terminate frequency by f_T. The upper frequency will determine the minimum sampling interval by Nyquist's or Shannon's criteria as

$$\Delta t = \frac{1}{2f_u} .$$

Then equation (55) can be written in summation form as

$$y_k = \Delta t \sum_{\ell=-N_d}^{N_d} h_\ell x_{k-\ell} , \tag{60}$$

$(k = N_d, N_d + 1, \ldots, (N - N_d),$

where

$$\begin{aligned} y_k &= y(k\Delta t) \\ h_\ell &= h(\ell \Delta t) \\ x_{k-\ell} &= x[(k-\ell)\ \Delta t] \end{aligned} \tag{61}$$

and

$$N = T/\Delta t.$$

The limit of summation $\pm N_d$ is dictated by the tolerance of error in the filter frequency response. Let us define the measure of error [IV-12] as

$$\epsilon(f,N_d) = H(f) - H(f,N_d), \tag{62}$$

where $H(f,N_d)$ is the N_d-term truncation of the infinite series representation of $H(f)$. It has been determined empirically that for the tolerance

$$0.5\% < \epsilon < 1\% \tag{63}$$

the minimum number required is given by

$$\min(N_d) = \frac{5f_u}{4(f_T - f_c)} , \tag{64}$$

with

$$f_u > 2f_T .$$

This shows that the sharper the roll-off rate in the filter, the greater the number of digital samples needed for a fixed accuracy tolerance. Figure IV.5 shows the phase and gain function of the Martin-Graham low-pass filter with f_c = 0.8 Hertz, f_T = 1.0 Hertz and N_d = 39. The figure clearly shows that there is only negligibly small phase distortion and that the gain is almost exactly as desired.

IV-4. EXPERIMENTAL AND COMPUTED RESULTS

To verify the theory that the probability density of wind component variations can be approximated by the crossed-beam technique, and to test the applicability of the data conditioning and handling methods described in the last two chapters, some computer-processed results of actual crossed-beam test data recorded in the lower atmosphere are presented in this chapter.

The field tests were carried out by the Colorado State University at Boulder, Colorado. A schematic crossed-beam test arrangement is illustrated in Figure IV.6. The detailed test site topography, geometry of the photodetectors, and meteorological conditions were reported in references IV-1 and IV-2.

The light source is the natural scattered radiation in the visible spectral range. A block diagram of the crossed-beam detection system is shown in Figure IV.7. Essentially, the incident radiation in the field of view of the telescope (0.5 degree) is focused on a photodetector (silicon diode). The radiation power is converted into voltage in proportion to its power. The fluctuating voltage is electronically separated into the d.c. and a.c. components with a time-constant of 100 seconds. In addition, a low-pass and high-pass filter of 0.01 Hz and 3 Hz, respectively, are set in the recording chain. Both a.c. and d.c. signals, together with the wind speed and direction obtained by anemometers, are recorded on an analog magnetic tape. More details of the optics and electronics, and associated signal/noise analyses were discussed in reference IV-3.

We shall present and discuss two test runs (I and II). The pertinent information is summarized in Table IV-1. The top view of the photometer arrangements and the probabilities of wind directions for these two runs are shown, respectively, in Figures IV.8(A) and (B). It can be seen that the wind direction was fairly constant during the measurements for both runs. For comparisons, anemometers were also mounted on a meteorological tower which was located between two lines of sight of the photometers (Figure IV.6).

The analog time histories of the a.c. signals are first digitized at a rate of 80 samples per second. These digital time histories are then averaged every 10 samples to reduce the sampling rate to 8 samples per second by the sample reduction method discussed in section IV-3. The purpose of the operation is to reduce the quantization errors due to the analog/digital conversion. These reduced digital time histories and their time derivatives are then used to evaluate the cross-correlations. Since the time histories are too long to be stored in their entirety in the computer, this evaluation is performed by a specially devised computer logic for piecewise correlation [IV-14, -15, and -16]. In short, a long time history of length T is to break into m shorter pieces of equal length $\triangle T$; $T = m \triangle T$. Each short piece of data is then processed to obtain a "piecewise" cross-correlation. These "piecewise" cross-correlations are sequentially averaged by a recursion formula to obtain the accumulative cross-correlation which is equal to the cross-correlation evaluated directly from the entire time history. By so doing, the computer needs only to store a time history of length $\triangle T$. In processing the test runs I and II, the piece length $\triangle T$ = 450 seconds, the maximum time lag τ_{max} = 50 seconds and the increment in time lag $\triangle\tau$ = 0.25 second.

Figure IV.9 shows the cross-correlation of the photometer outputs for run I with the lower and upper frequency cut-off, 0.01 Hz and 3.0 Hz, respectively. The extremely erratic curve indicates clearly that the upper frequency of 3 Hz is too high. An examination of the corresponding gain shows that a narrow-band noise component exists at 1.25 Hz. So, to smooth the cross-correlation, the noise component has to be filtered out. Figures IV.10 through IV.12 show three different cases of cross-correlations $R_{xy}(\tau)$ and $R_{xy}^{(2)}(\tau)$ of the outputs and their time derivatives of run I, which are obtained by using three different roll-offs in the digital filtering. All three have the same terminate frequency f_T = 1.0 Hz, while the cut-off frequencies, f_c, equal 0.8, 0.6 and 0.4 Hz, respectively. Also shown in these figures are the 90-percent confidence limits of $R_{xy}(\tau)$ and $R_{xy}^{(2)}(\tau)$ as denoted by $\overline{\overline{R_m(\tau)}}$ and $\overline{\overline{R_m^{(2)}(\tau)}}$, respectively [IV-15]. All three $R_{xy}(\tau)$ curves are much smoother compared to the curve in Figure IV.9, and there is only one peak in $R_{xy}(\tau)$ around τ = 10 seconds, which exceeds the confidence limit at least by two times. This means that only this peak has the sufficient statistical significance, and that the rest of the curve is due to nothing but noises which have not been completely

eliminated. Therefore, only the portion of $R_{xy}^{(2)}(\tau)$ which corresponds to this significant peak should be selected with sufficient statistical confidence. For easy identification, these portions of $R_{xy}^{(2)}(\tau)$ are shaded.

Figure IV.13 presents the statistical errors of $\overline{\overline{\delta R_m}}$ of the cross-correlations $R_{xy}(\tau)$ versus the inverse square root of the integrating time $T = mt$. The statistical error is defined as the average of the confidence limit $\overline{\overline{R_m(\tau)}}$ integrated over the time lag from $-\tau_{max}$ to $+\tau_{max}$ [IV-14]. For statistical stationary processes, the theory shows that these curves should approximate a straight line drawn through the origin of the coordinates, and that the slope of the straight line gives the inverse square root of an equivalent bandwidth B_{eff}, as if the associated spectrum were a white noise spectrum [IV-16]. The figure shows the equivalent bandwidth $B_{eff} = 0.182$ Hz for run I. It is also noted that the statistical error for $f_c = 0.8$ Hz is the smallest, while the error for $f_c = 0.4$ Hz is the largest. This is expected, since the error is proportional to the inverse square root of the bandwidth used.

Figures IV.14 through IV.16 show the gains $G_{xy}(f)$ and $G_{xy}^{(2)}(f)$ corresponding to Figures IV.10 through IV.12. Table IV-2 summarizes the approximate power law for each gain and the corresponding increase in exponent from $G_{xy}(f)$ to $G_{xy}^{(2)}(f)$. For stationary processes, the increase in the exponent of the power from $G_{xy}(f)$ should be 2 (see equation (46)). Table IV-2 indicates that the case with $f_c = 0.4$ Hz and $f_T = 1.0$ Hz gives a power law closest to that for stationary processes. It also implies that the components of the photometer outputs between 0.4 Hz and 1.0 Hz is less stationary than those between 0.01 Hz and 0.4 Hz. To further demonstrate the nonstationarity, $G_{xy}^{(2)}(f)$ and $f^2\, G_{xy}(f)$ for each case are plotted in Figures IV.17 through IV.19. Comparing of these figures also shows that the best agreement between $G_{xy}^{(2)}(f)$ and $f^2\, G_{xy}(f)$ is for the case with $f_c = 0.4$ Hz.

Finally, we come to check our ultimate goal, i.e., to retrieve optically the turbulent wind statistics. Figure IV.20 shows the normalized probability density of wind component variations (normal to both beams) deduced from the optical cross-beam measurements, as well as from the anemometer readings. Clearly, the most probable wind component obtained optically is within 5 percent of that obtained by the direct measurement. The rms of the wind component variations obtained optically is slightly larger than that by the anemometer. The best agreement between them again is offered by using $f_c = 0.4$ Hz and $f_T = 1.0$ Hz. It is also noted that the probability density obtained by the crossed-beam technique is somewhat skewed to higher wind component compared to that by the anemometer. The reason for this skewness is still being investigated. Figure IV.21 shows another comparison of the probability densities obtained both optically and directly for run II with $f_\ell = 0.01$ Hz and

f_u = 0.3 Hz. Once again, the crossed-beam measurement yields very accurately the most probable wind component. The rms of the wind component variations is about 25 percent less than that by the anemometer. The optical probability density also shows a similar skewness to higher wind components.

IV-6. CONCLUSIONS

The crossed-beam technique employing the natural scattered radiations is shown to be capable of remote detection of the wind component variations normal to the two light beams. A theoretical relationship is derived which approximates the probability density of the wind component variations in terms of the measurable cross-correlation of the photometer outputs under three fairly realistic assumptions on the atmospheric turbulence and wind statistics. Specifically, it is shown that the probability density of the wind component is directly proportional to the temporal cross-correlation of the first time derivatives of the light intensity fluctuations multiplied by the time lag introduced between the two time histories. The moments of the wind component variations can be easily evaluated once the probability density is obtained by the optical crossed-beam technique.

Because of the very low signal-to-noise ratio for the time histories intrinsic to this type of remote detection, the digital analysis is far more preferable to analog analysis for higher statistical accuracy. Furthermore, because of the necessity to use the time derivatives of the photometer outputs which are approximated by the finite difference scheme, the sample reduction method is used to reduce the quantization error by about 30 percent. More importantly, a suitable digital filtering should be used to filter out the higher frequency noises which are weighted by a factor of frequency square due to the necessity of using the time derivatives. The digital filtering process is fairly time-consuming even for fast computers, and the computation time required is shorter for slower roll-off in the frequency response function of the low-pass filter. Three different types of roll-offs are studied to see their effects on the evaluations of the cross-correlation and the corresponding spectral densities. These roll-offs have the same terminate frequency of 1.0 Hz, while the cut-off frequencies are 0.8 Hz, 0.6 Hz and 0.4 Hz, respectively.

Actual field tests have been carried out in the atmosphere at Boulder, Colorado. Two lines of sight have been crossed about 61 meters from the ground. The photometer signals were processed by a special piecewise computer program, together with two subroutines for applying the sample reduction method and for the digital filtering. The optically measured probability densities of wind component variations were found

to be in reasonable agreement with those measured directly by the conventional anemometers mounted on a meteorological tower at the same crossing height. The most probable wind components obtained by the crossed-beam technique are within 5 percent of that obtained by the anemometer. The root mean squares of the wind component variations obtained by the former for two different tests are within 5 and 25 percent, respectively, of those measured by the latter. For still-unknown reasons, the probability density curve obtained by the optical means is relatively skewed to higher wind speeds as compared to that from the anemometer. It is also found that the best agreement in the probability density of wind components was obtained by using the slowest roll-off, i.e., f_c = 0.4 Hz and f_T = 1.0 Hz. This strongly suggests that the best frequency range might be between 0.01 Hz to 0.5 Hz for these tests. Theoretical considerations predict that the optimum cut-off frequency f_c will be determined by two factors: (a) the maximum wind component to be expected U_{max} and (b) the smallest atmospheric eddy size L_{min} which will preserve sufficiently its characteristics over the transmission between two light beams. Specifically, $f_c = U_{max}/2\pi L_{min}$. This gives f_c = 0.318 Hz for U_{max} = 20 m/sec (run I) and L_{min} = 10 meters [IV-8], which is close to the experimentally determined value of 0.4 Hz. More experimental results are desirable before we can establish conclusively an optimum frequency range and the shape of frequency response function of the digital filtering with minimum required computation time.

The analytical results and data-processing methods developed for the atmospheric turbulence measurement can be applied to measure turbulence in other fluid flow problems as well. The optical technique is particularly advantageous over the hot-wire and the like in measuring the flow speed and turbulence intensity of high-temperature, chemically reacting or supersonic flow fields associated with rocket engine plume, boiling phenomena in nuclear reactors, plasma, etc. All of these flow fields, at the present time, defy accurate and free-from-interference measurements by conventional direct-sensing instrumentations.

TABLE IV-1. TEST RUN SPECIFICATION

SPECIFICATION	RUN I	RUN II
BEAM SEPARATION	93 meters	117 meters
CROSSING HEIGHT	51 meters	61 meters
ANEMOMETER LEVEL	62 meters	61 meters
BASELINE BETWEEN PHOTOMETERS	220 meters	220 meters
BEAM ELEVATION	45°	45°
BEAM AZIMUTH	4° to N.	14° to N.
MEASURING TIME:		
START	1:43 p.m.	11:01 a.m.
END	2:36 p.m.	12:03 a.m.
SKY CONDITION	clear	clear

TABLE IV-2. APPROXIMATE POWER LAWS OF GAINS OF PHOTOMETER OUTPUTS AND THEIR TIME DERIVATIVES

DIGITAL FILTER SETTING (Hz)		EXPONENT IN THE POWER LAW APPROXIMATION		INCREASE IN THE EXPONENT FROM
f_c	f_T	$G_{xy}(f)$	$G_{xy}^{(2)}(f)$	$G_{xy}(f)$ to $G_{xy}^{(2)}(f)$
0.8	1.0	-1.45	-0.25	1.20
0.6	1.0	-1.58	-0.22	1.36
0.4	1.0	-1.83	0	1.83

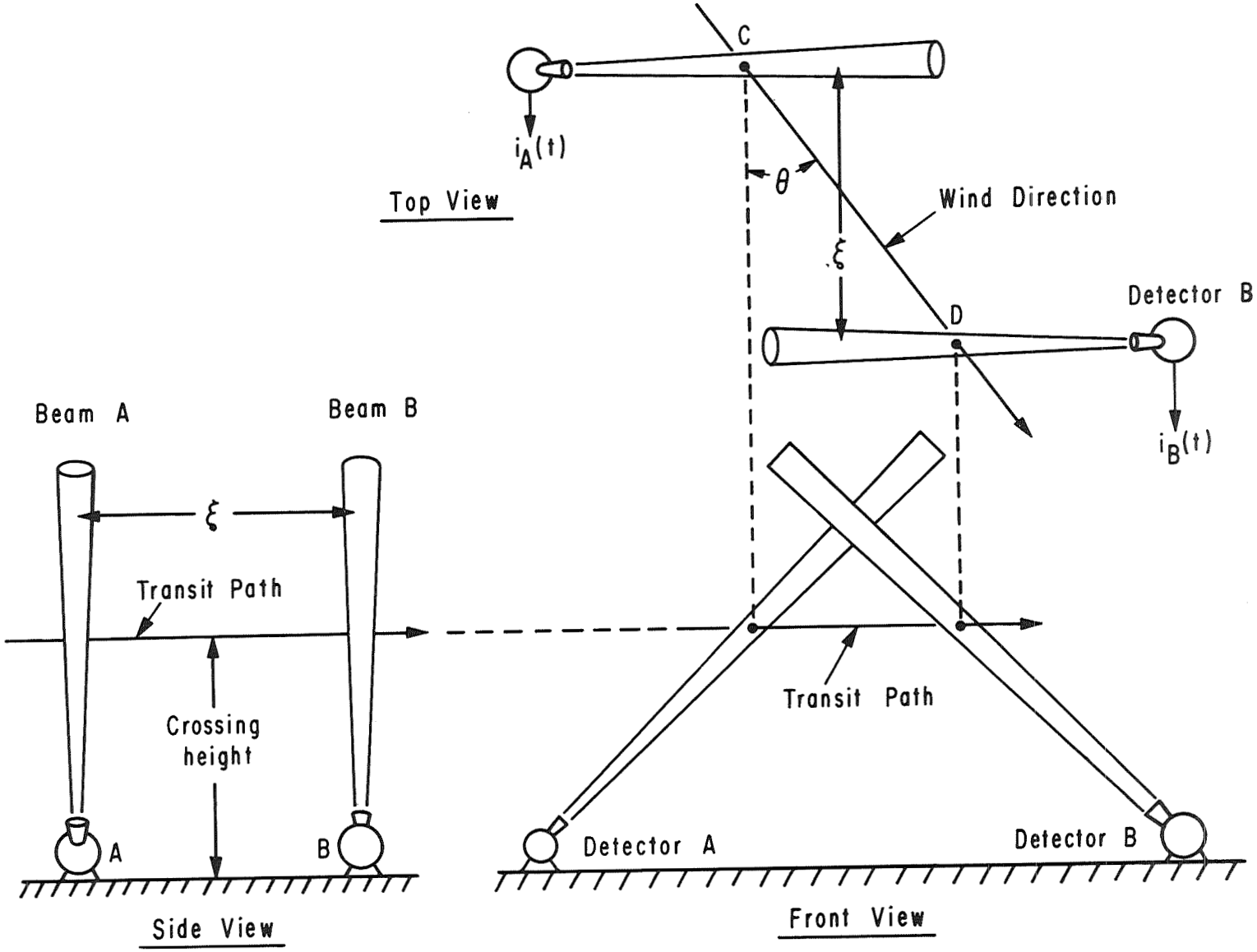

FIGURE IV.1. GROUND-BASED CROSSED-BEAM PHOTOMETER ARRANGEMENT

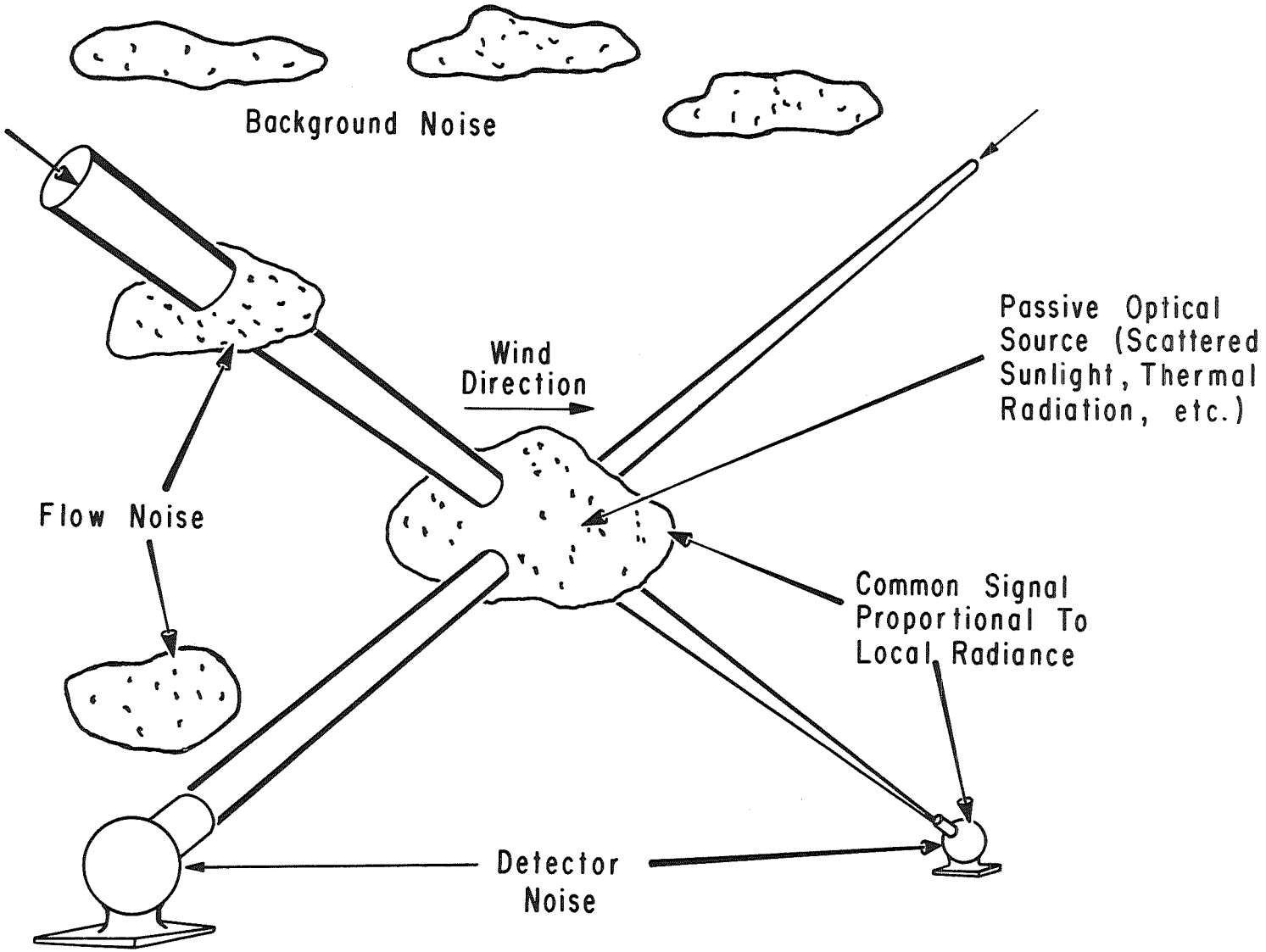

FIGURE IV.2. CROSSED-BEAM SIGNAL AND NOISE SOURCES

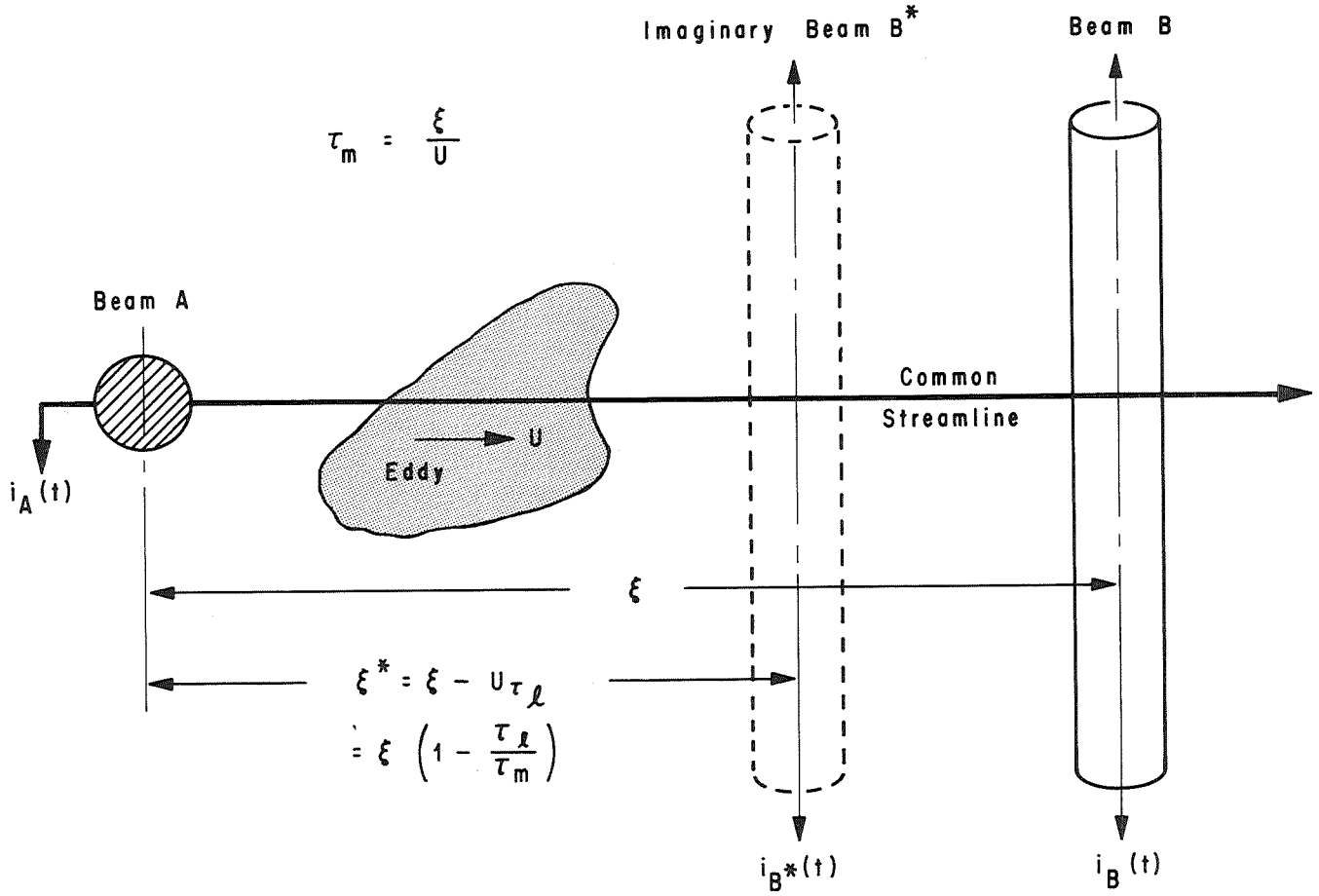

$$\overline{R}(\xi, \tau) \equiv \left\langle i_A(t)\, i_B(t+\tau, \xi) \right\rangle = \left\langle i_A(t)\, i_{B^*}(t, \xi^*) \right\rangle$$

FIGURE IV.3. INTERPRETATION OF IMAGINARY BEAM B*

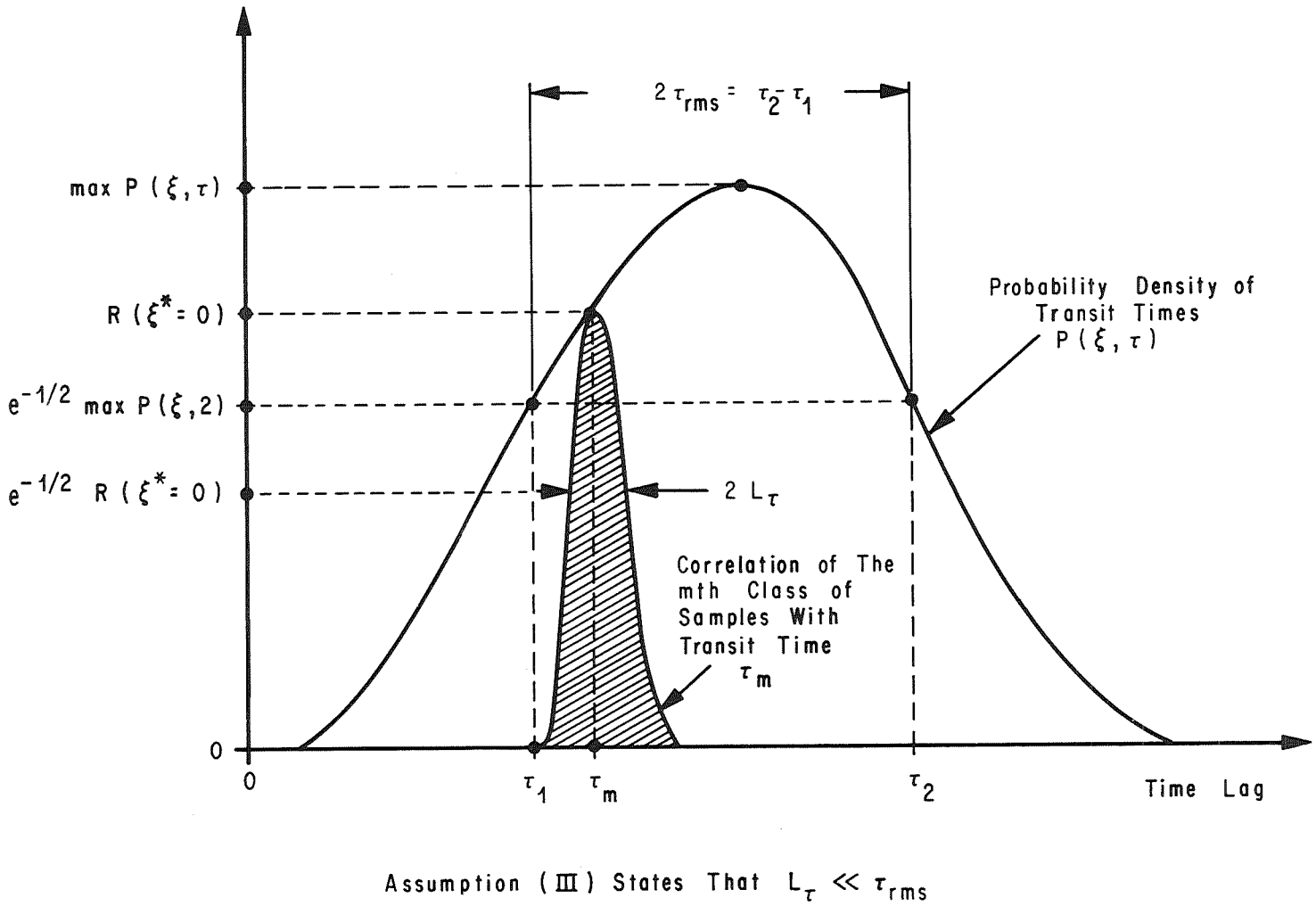

FIGURE IV.4. ILLUSTRATION OF THE ASSUMPTION

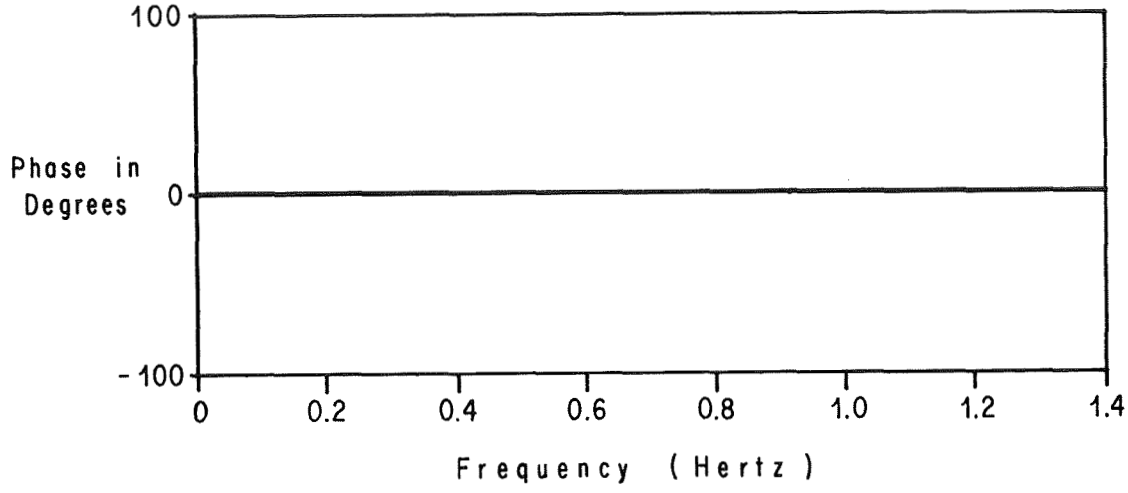

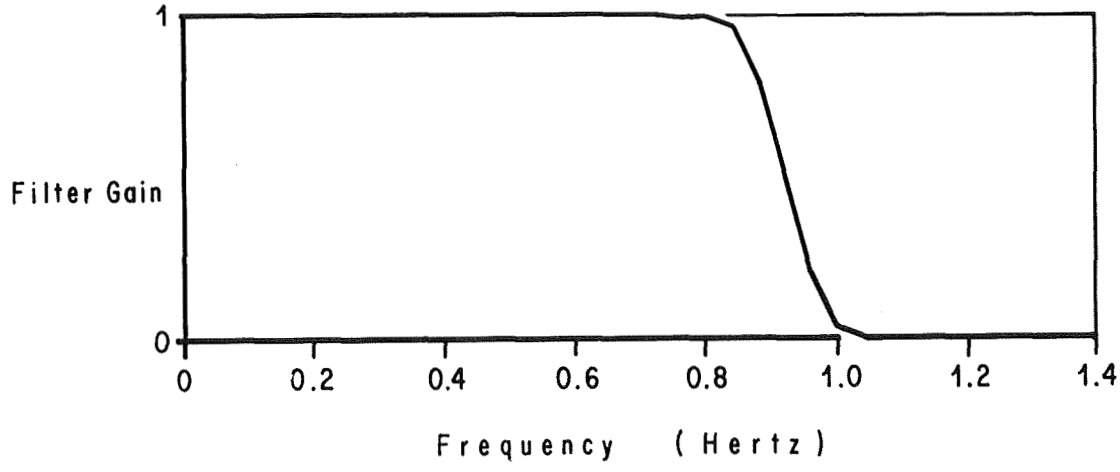

FIGURE IV.5. RESPONSE FUNCTION (PHASE AND GAIN)
OF THE MARTIN-GRAHAM LOW-PASS DIGITAL FILTER

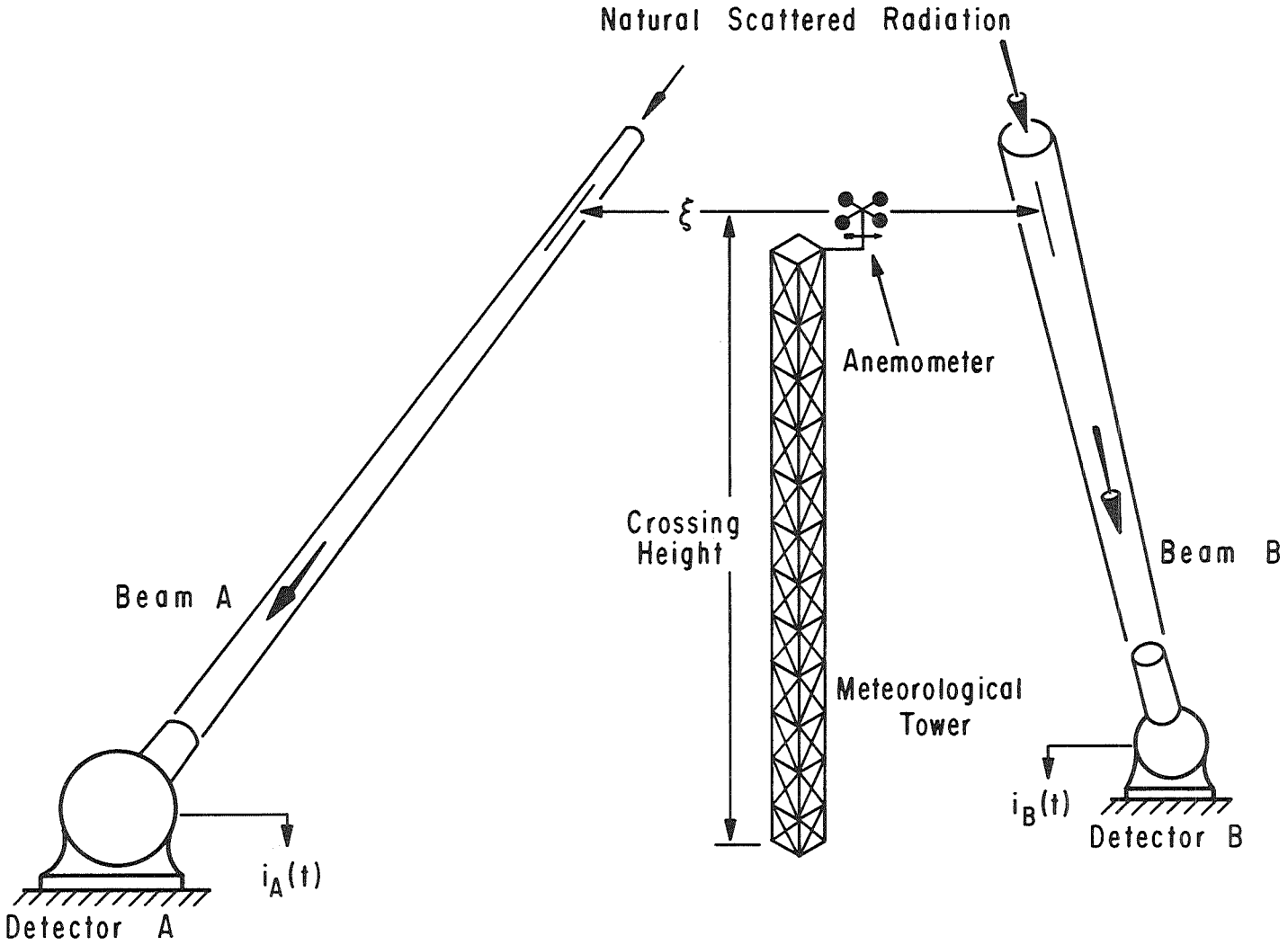

FIGURE IV.6. CROSSED-BEAM TEST ARRANGEMENT

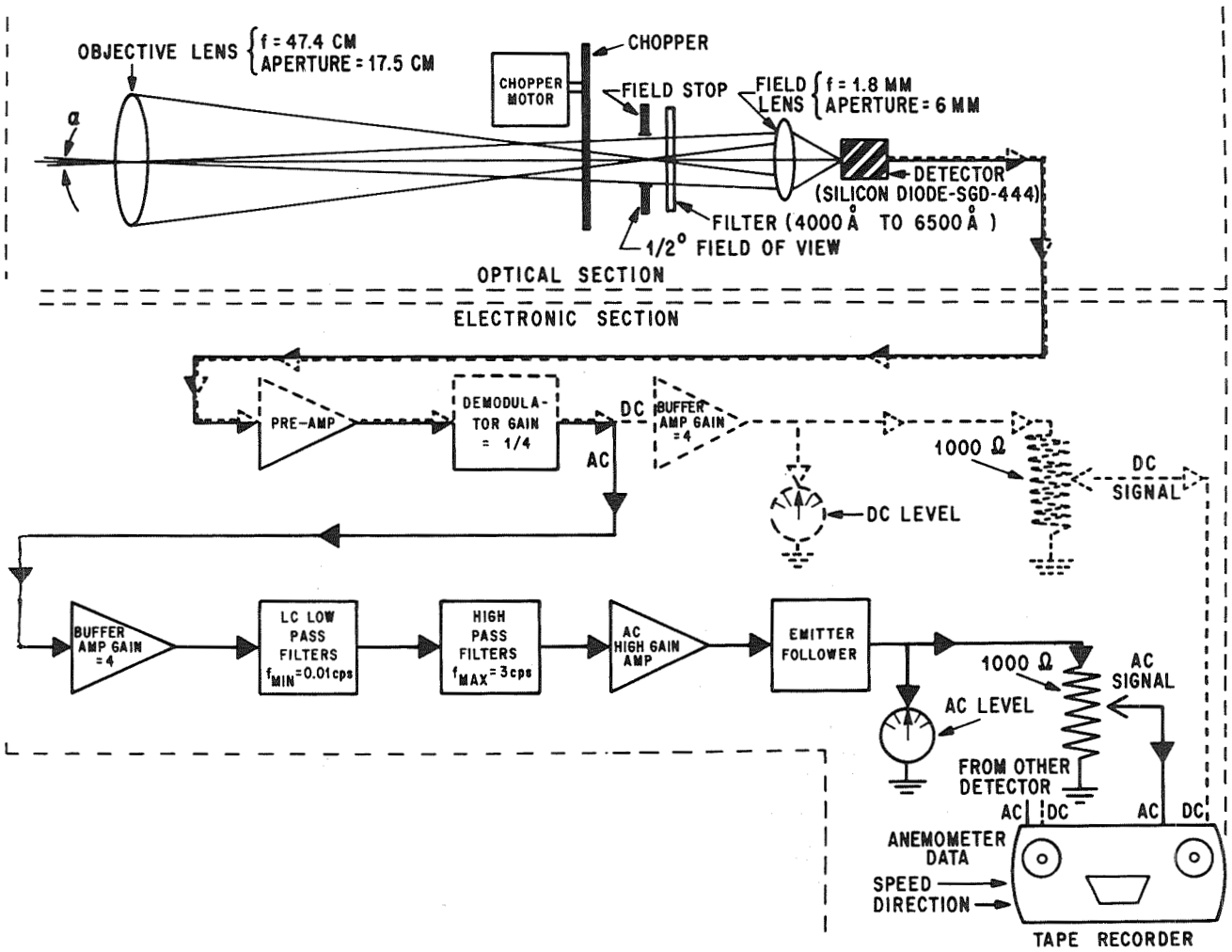

FIGURE IV.7. BLOCK DIAGRAM OF THE DETECTION STAGE

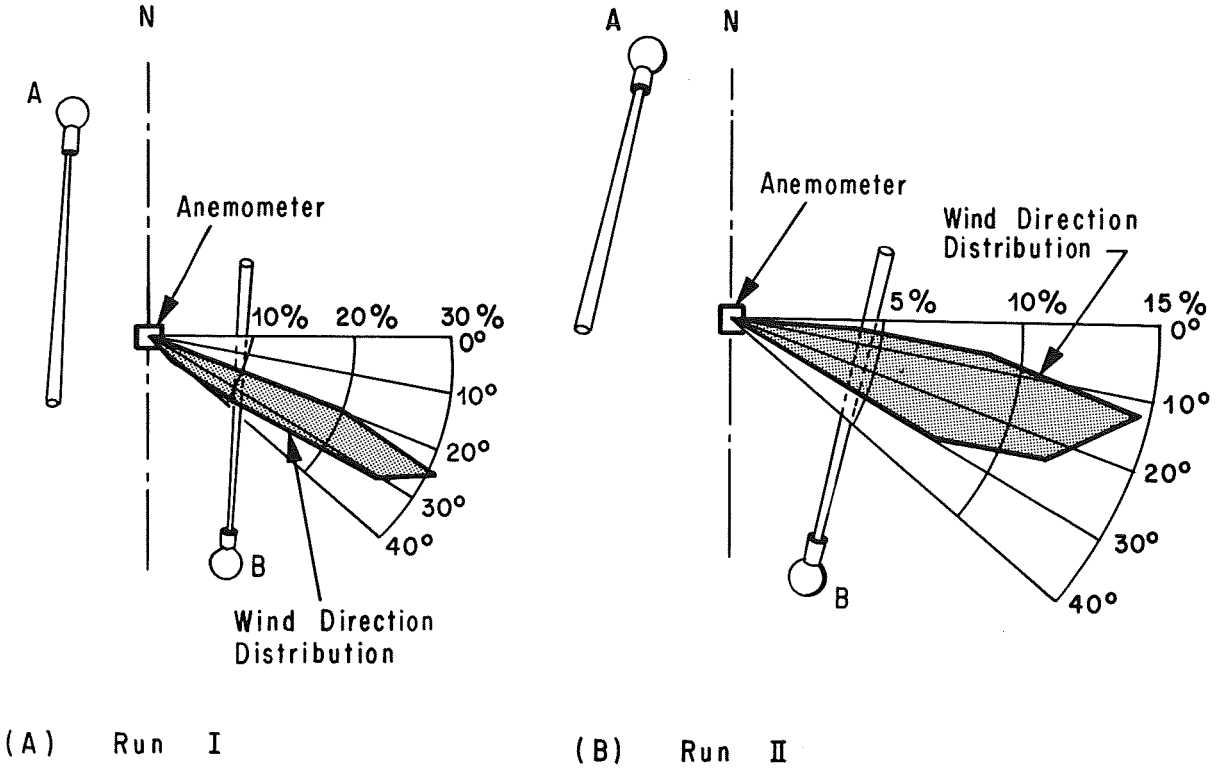

FIGURE IV.8. PROBABILITY OF WIND DIRECTIONS FOR TEST RUNS I AND II

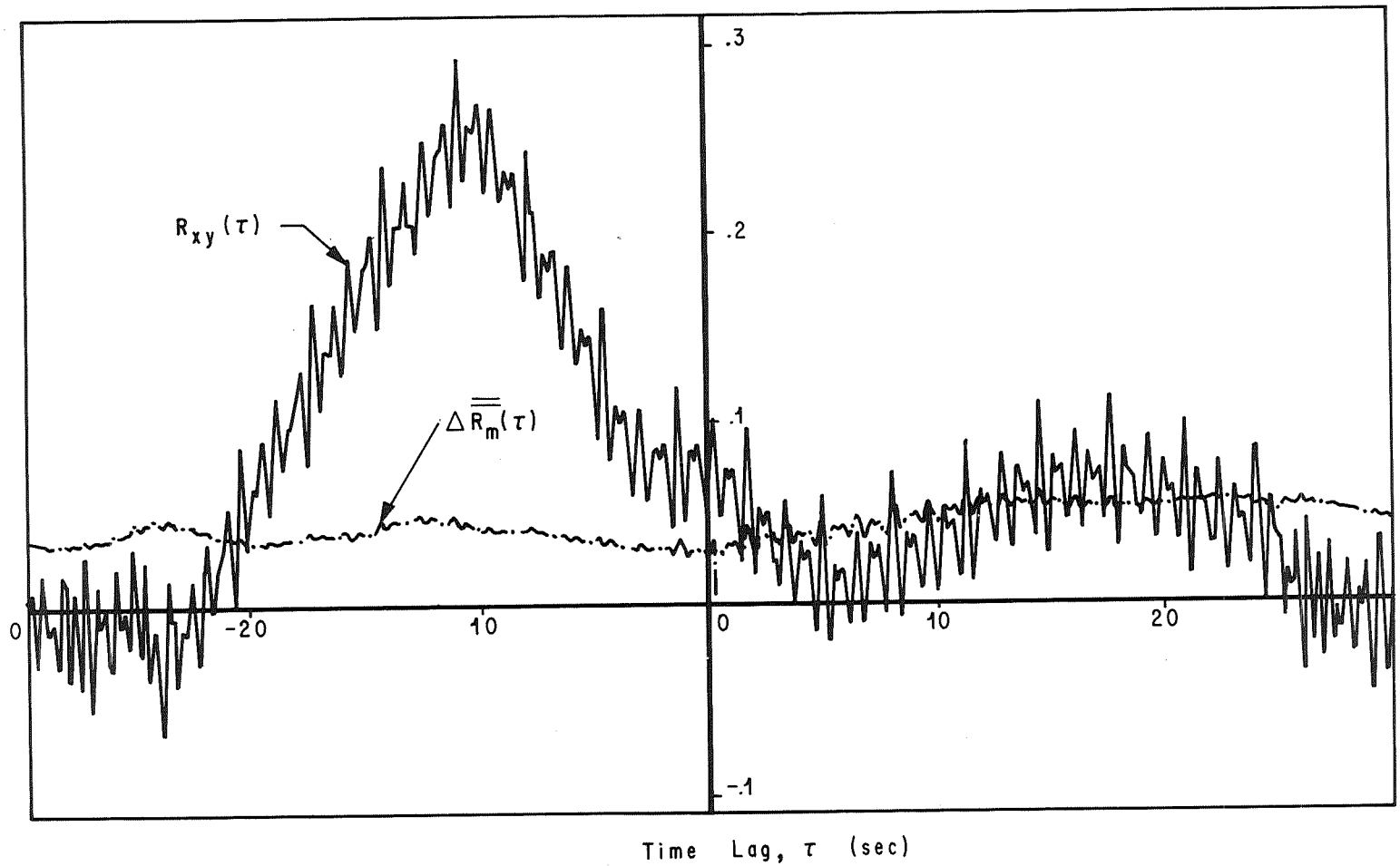

FIGURE IV.9. CROSS-CORRELATION AND CONFIDENCE LIMIT FOR f_l = 0.01 Hz and f_u = 3.0 Hz (RUN I)

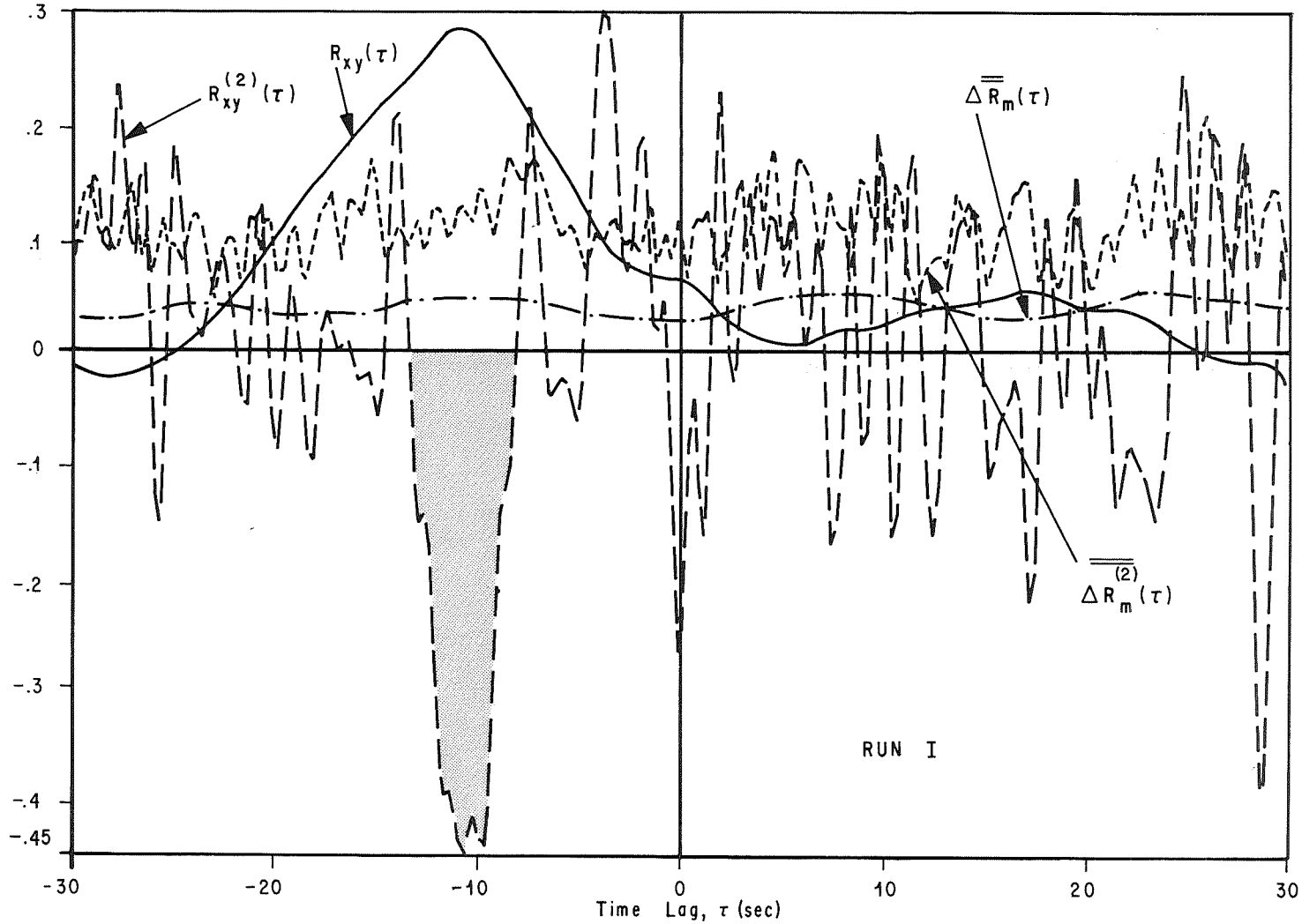

FIGURE IV.10. CROSS-CORRELATIONS AND CONFIDENCE LIMITS FOR f_c = 0.8 Hz and f_T = 1.0 Hz (RUN I)

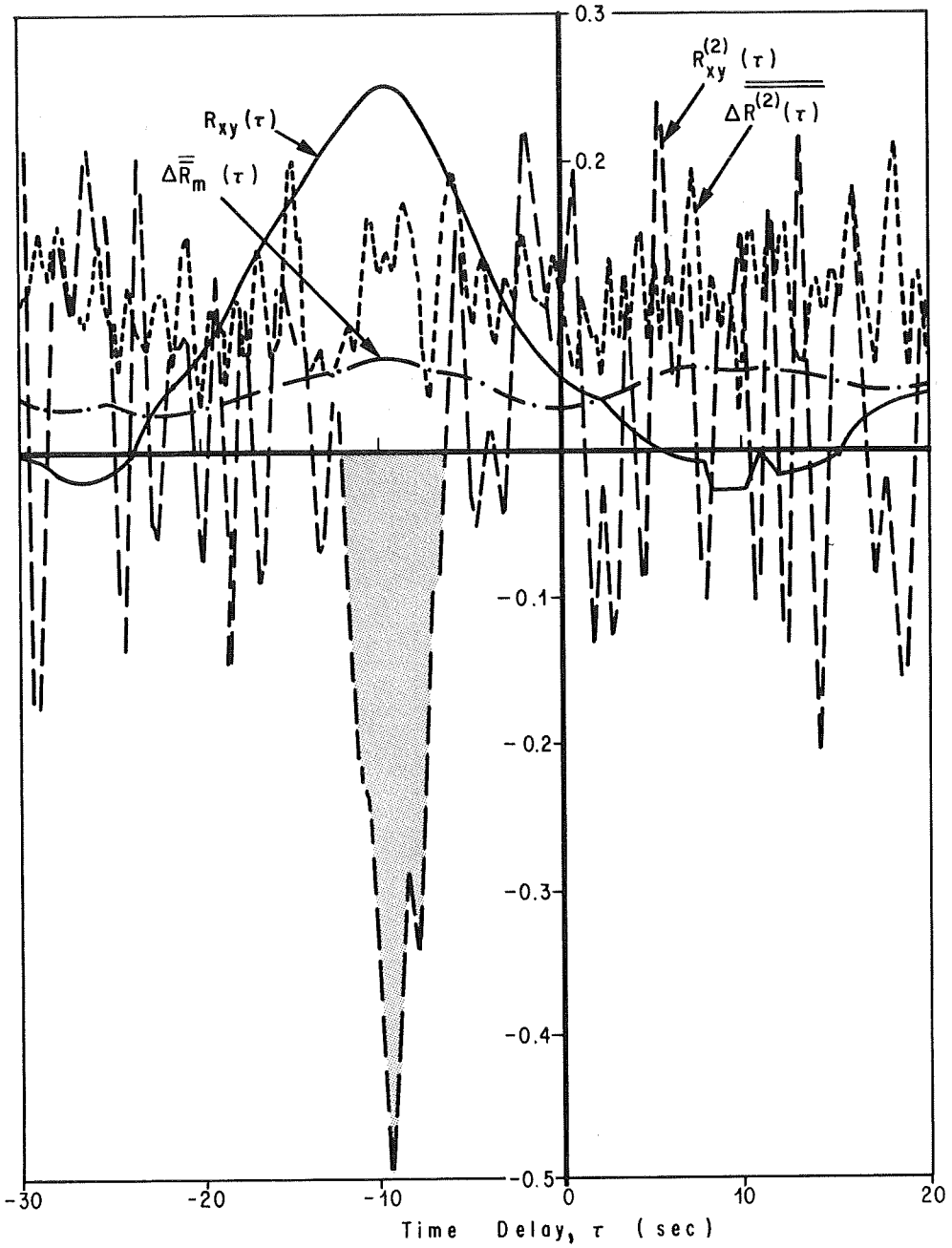

FIGURE IV.11. CROSS-CORRELATION AND CONFIDENCE LIMITS FOR f_c = 0.6 Hz and f_T = 1.0 Hz (RUN I)

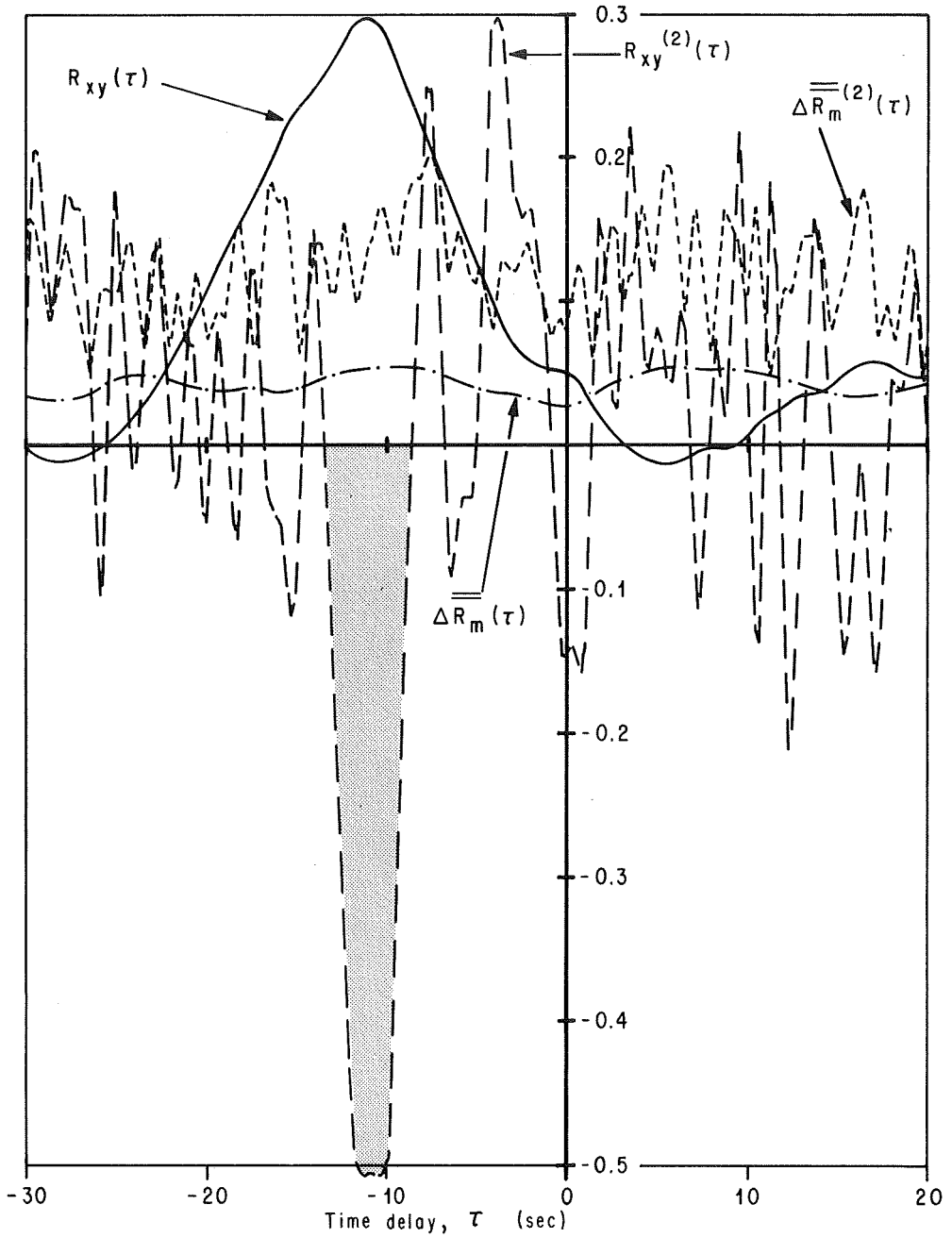

FIGURE IV.12. CROSS-CORRELATIONS AND CONFIDENCE LIMITS FOR f_c = 0.4 Hz AND f_T = 1.0 Hz (RUN I)

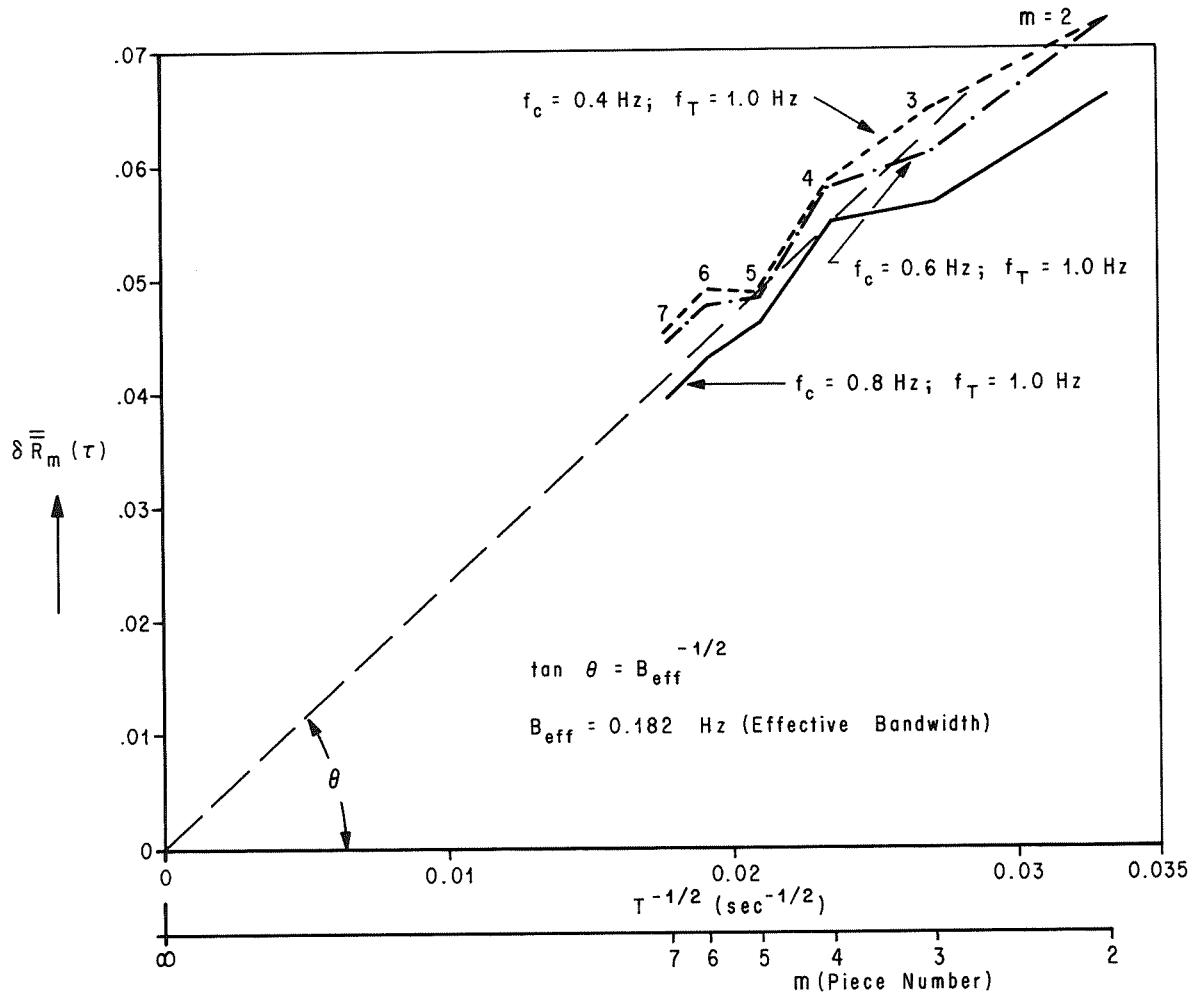

FIGURE IV.13. STATISTICAL ERROR OF CROSS-CORRELATION (RUN I)

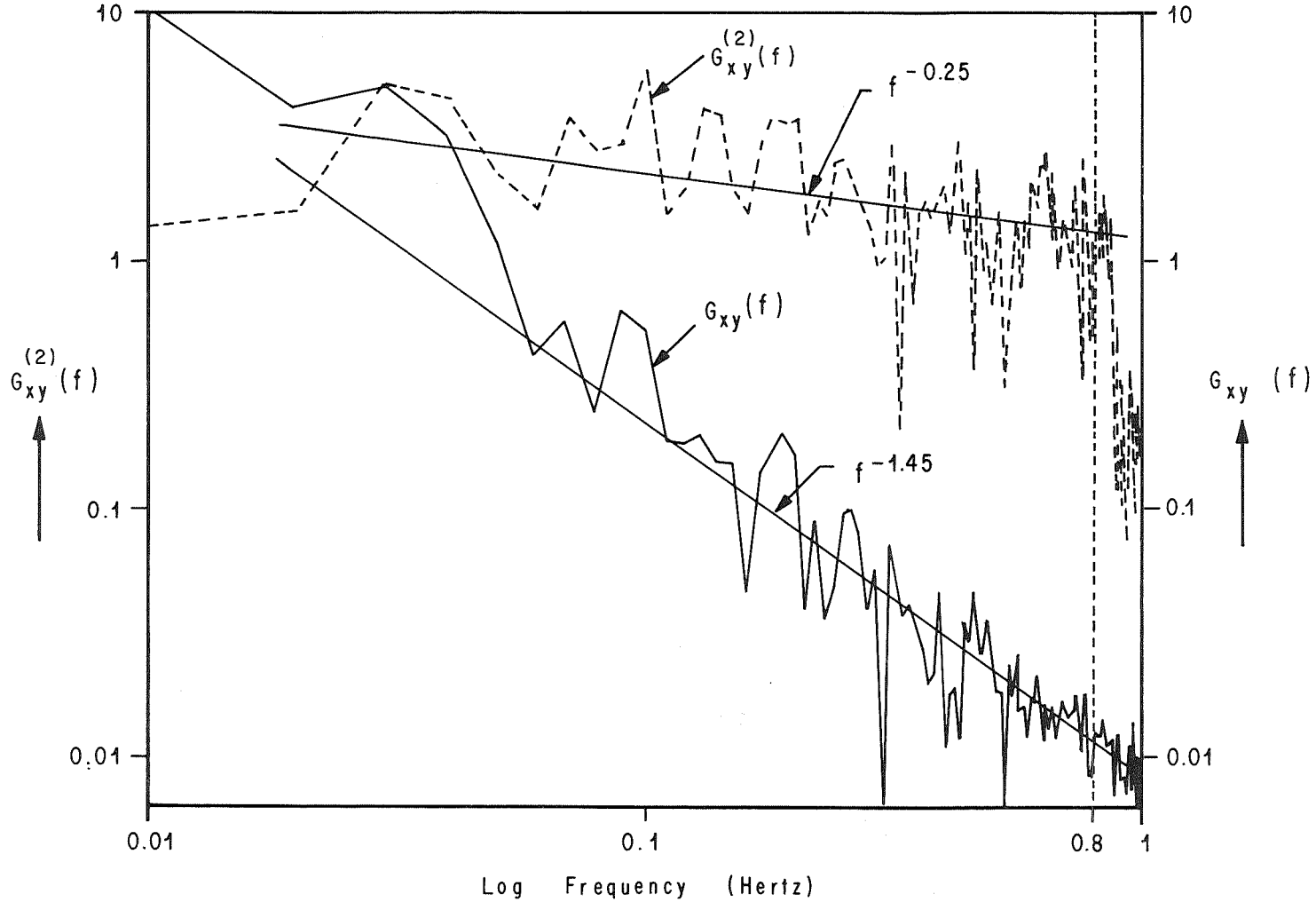

FIGURE IV.14. COMPARISON OF THE GAINS $G_{xy}(f)$ AND $G^{(2)}_{xy}(f)$ FOR f_c = 0.8 Hz and f_T = 1.0 Hz (RUN I)

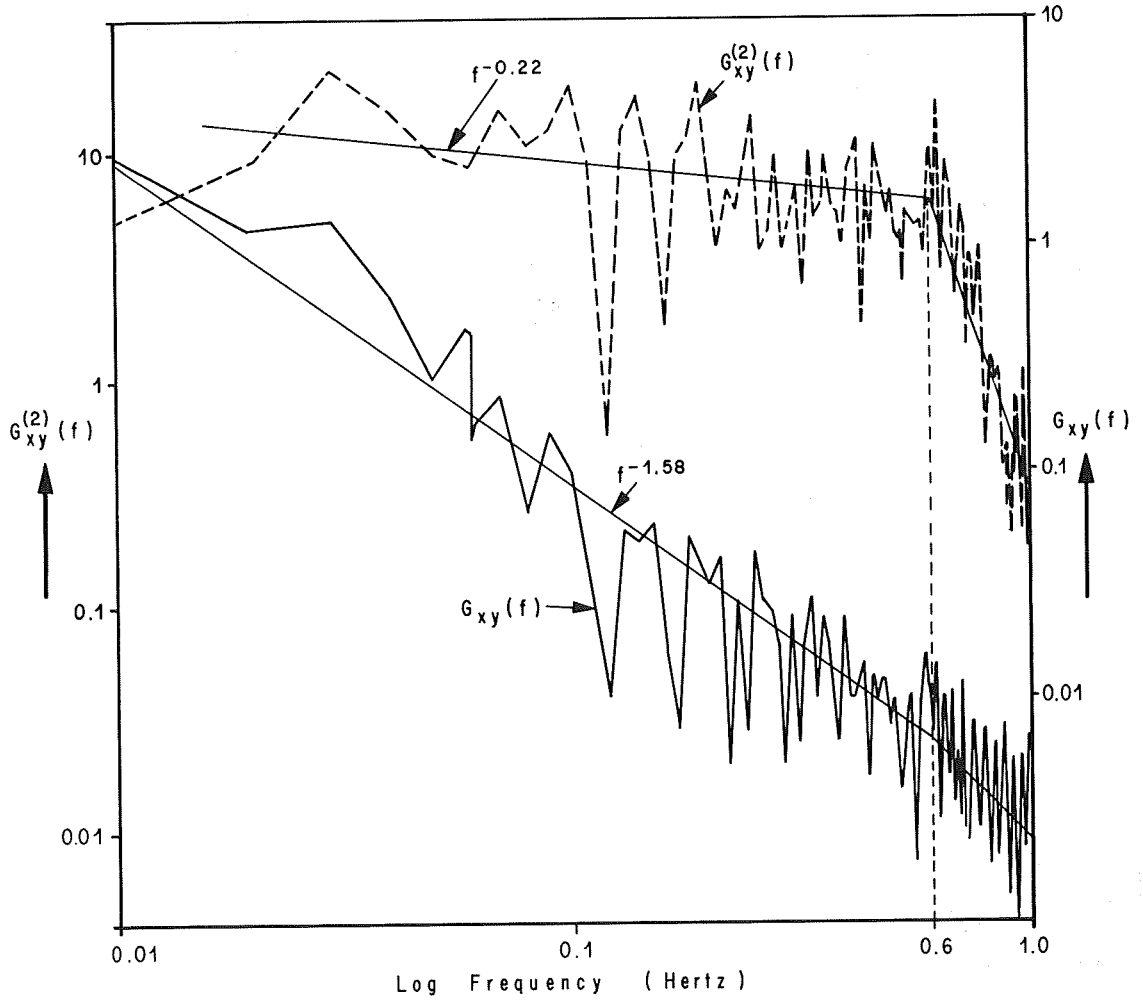

FIGURE IV.15. COMPARISON OF THE GAINS $G_{xy}(f)$ AND $G^{(2)}_{xy}(f)$ FOR f_c = 0.6 Hz and f_T = 1.0 Hz (RUN I)

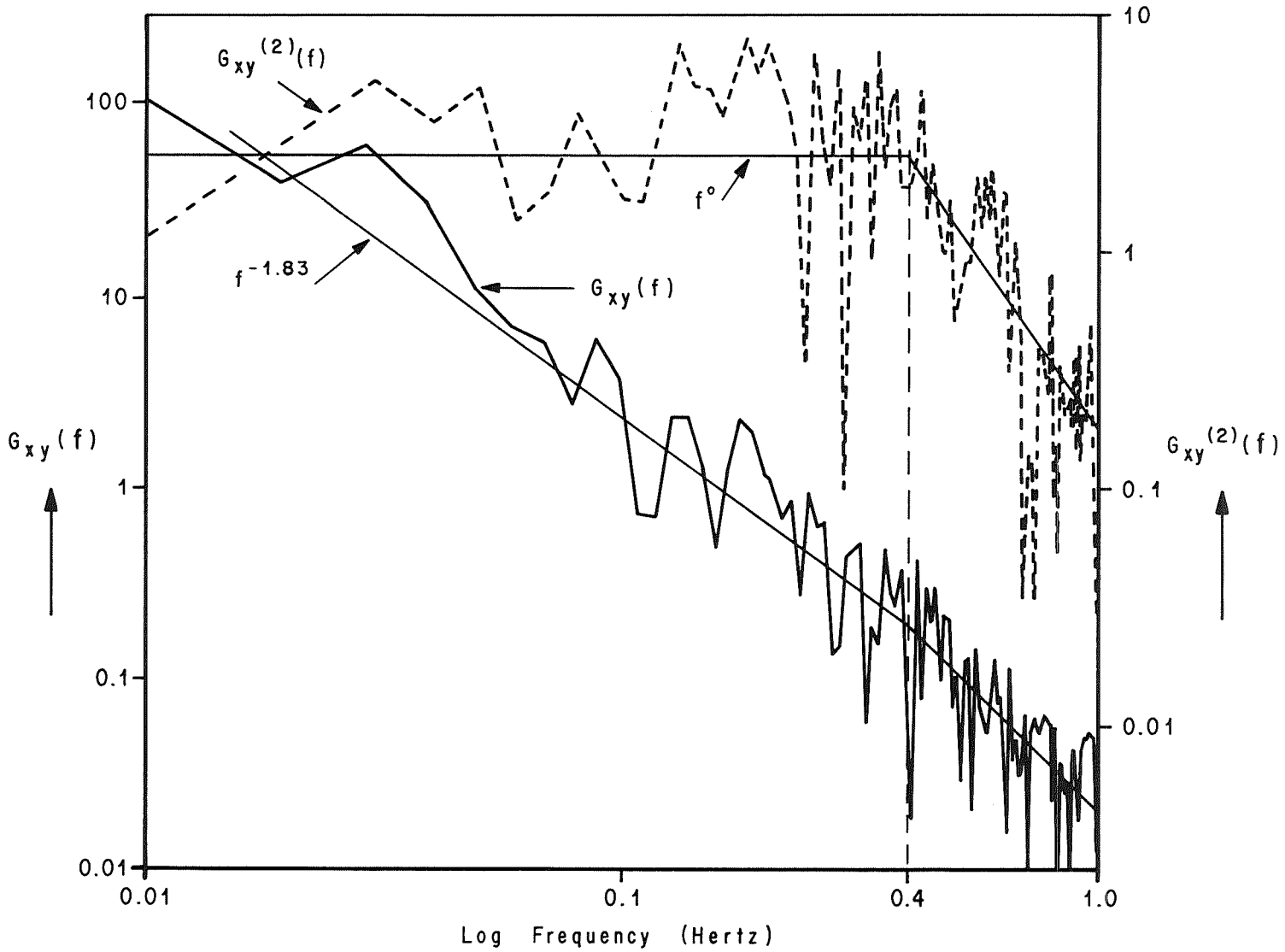

FIGURE IV.16. COMPARISON OF THE GAINS $G_{xy}(f)$ AND $G_{xy}^{(2)}(f)$ FOR f_c = 0.4 Hz AND f_T = 1.0 Hz (RUN I)

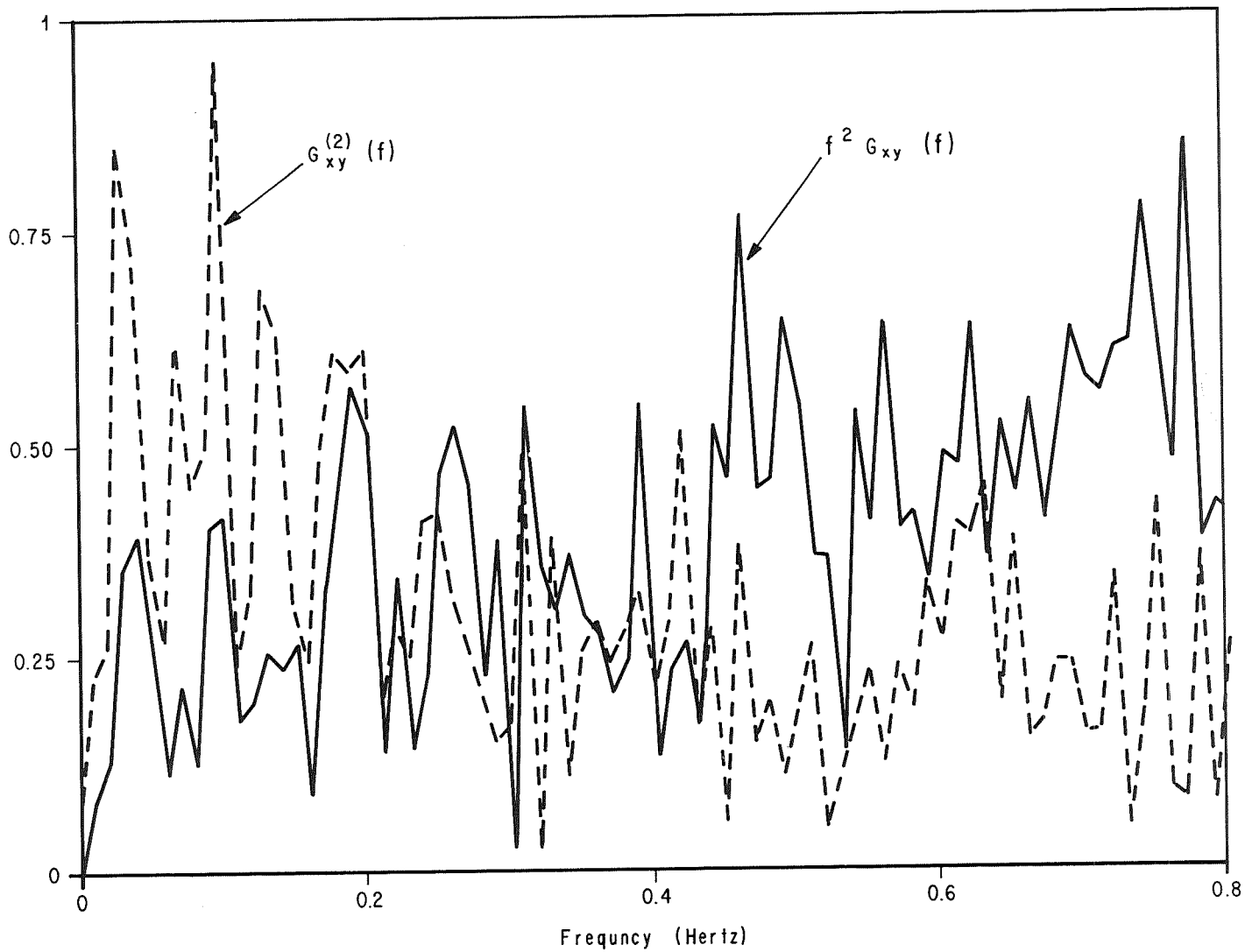

FIGURE IV.17. COMPARISON OF $G_{xy}^{(2)}(f)$ WITH $f^2 G_{xy}(f)$ FOR f_c = 0.6 Hz AND f_T = 1.0 Hz (RUN I)

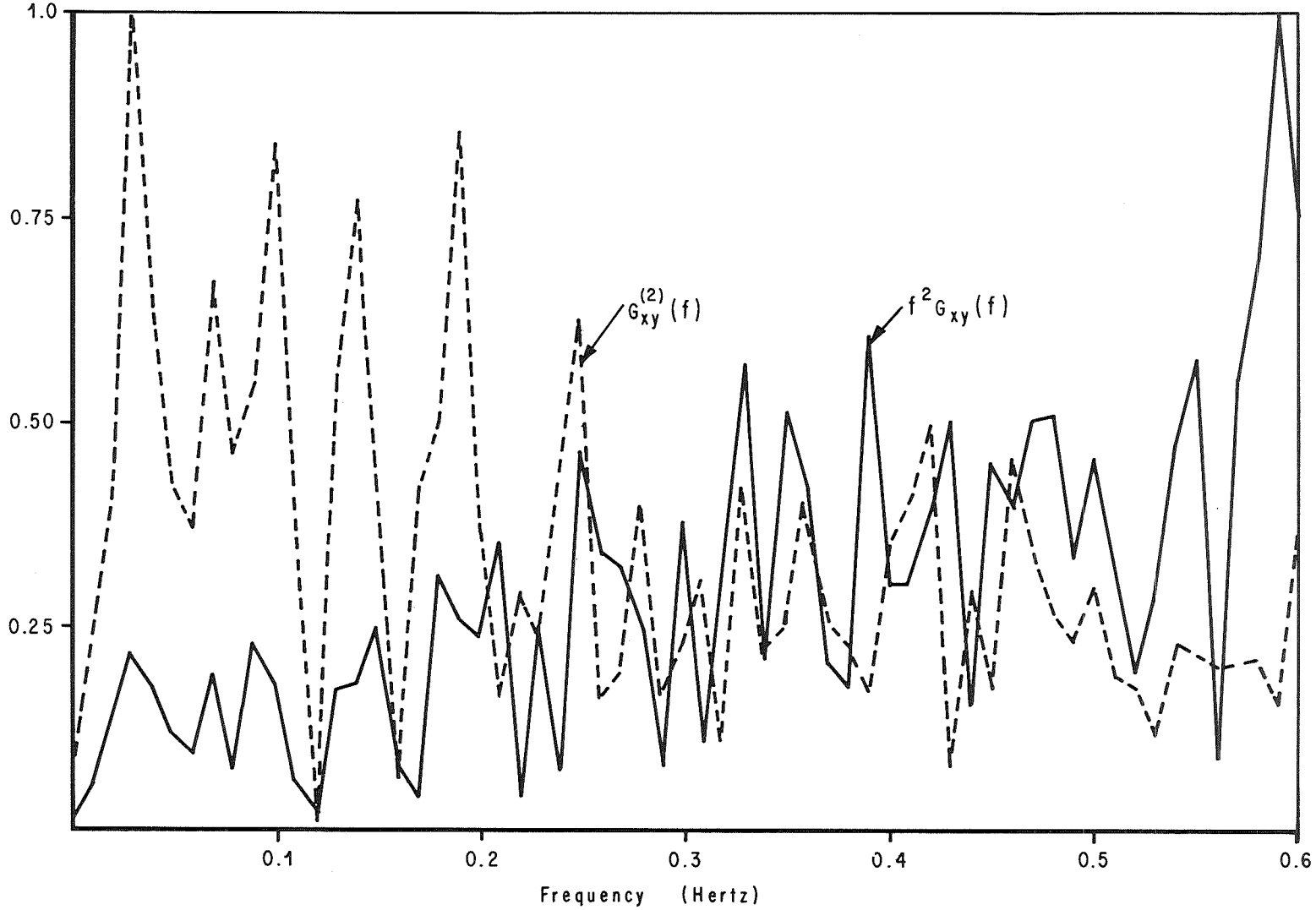

FIGURE IV.18. COMPARISON OF $G_{xy}^{(2)}(f)$ WITH $f^2\, G_{xy}(f)$ FOR f_c = 0.6 Hz AND f_T = 1.0 Hz (RUN I)

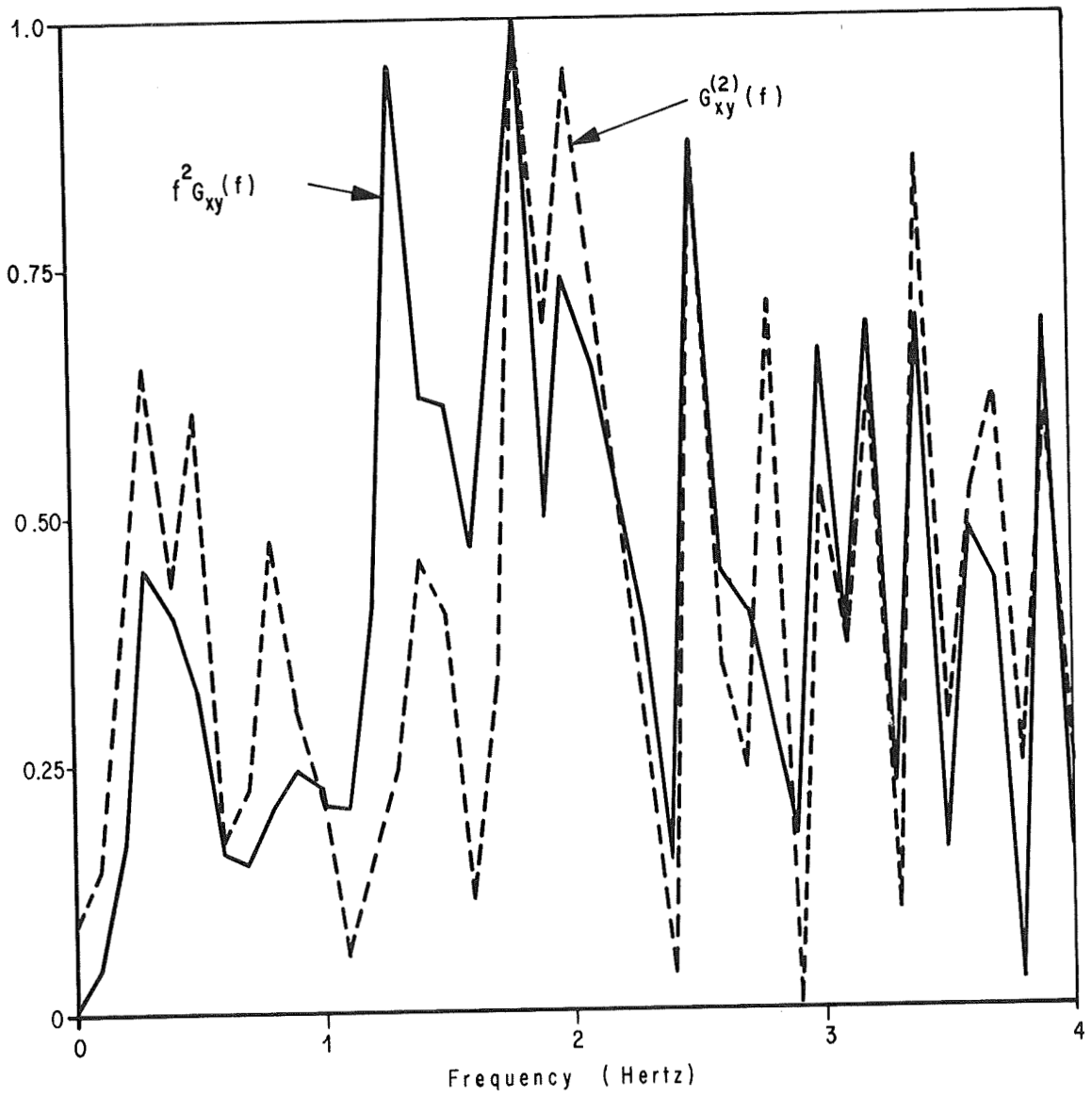

FIGURE IV.19. COMPARISON OF $G_{xy}^{(2)}(f)$ WITH $f^2 G_{xy}(f)$ FOR f_c= 0.4 Hz AND f_T = 1.0 Hz (RUN I)

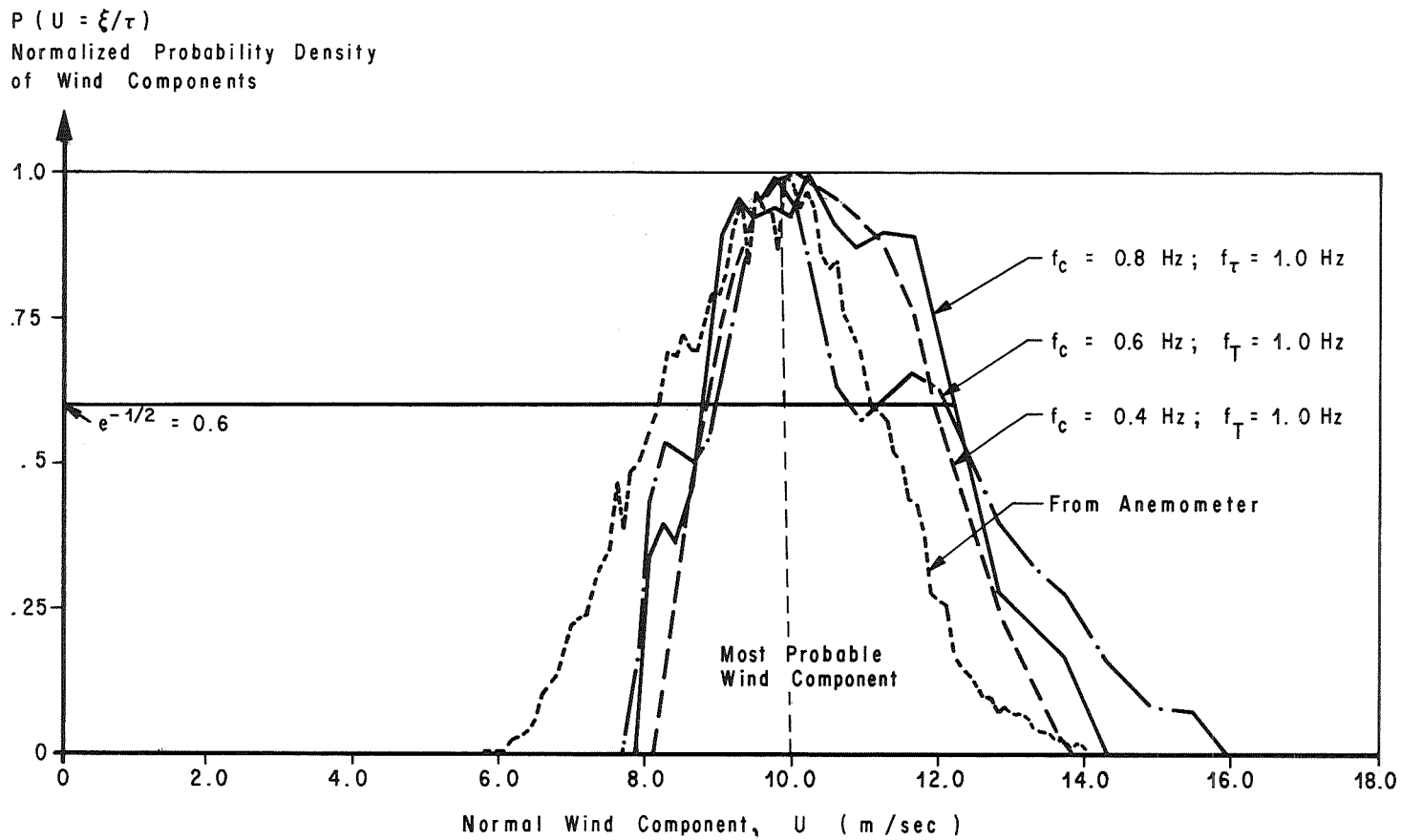

FIGURE IV.20. PROBABILITY DENSITY OF WIND COMPONENT VARIATIONS (RUN I)

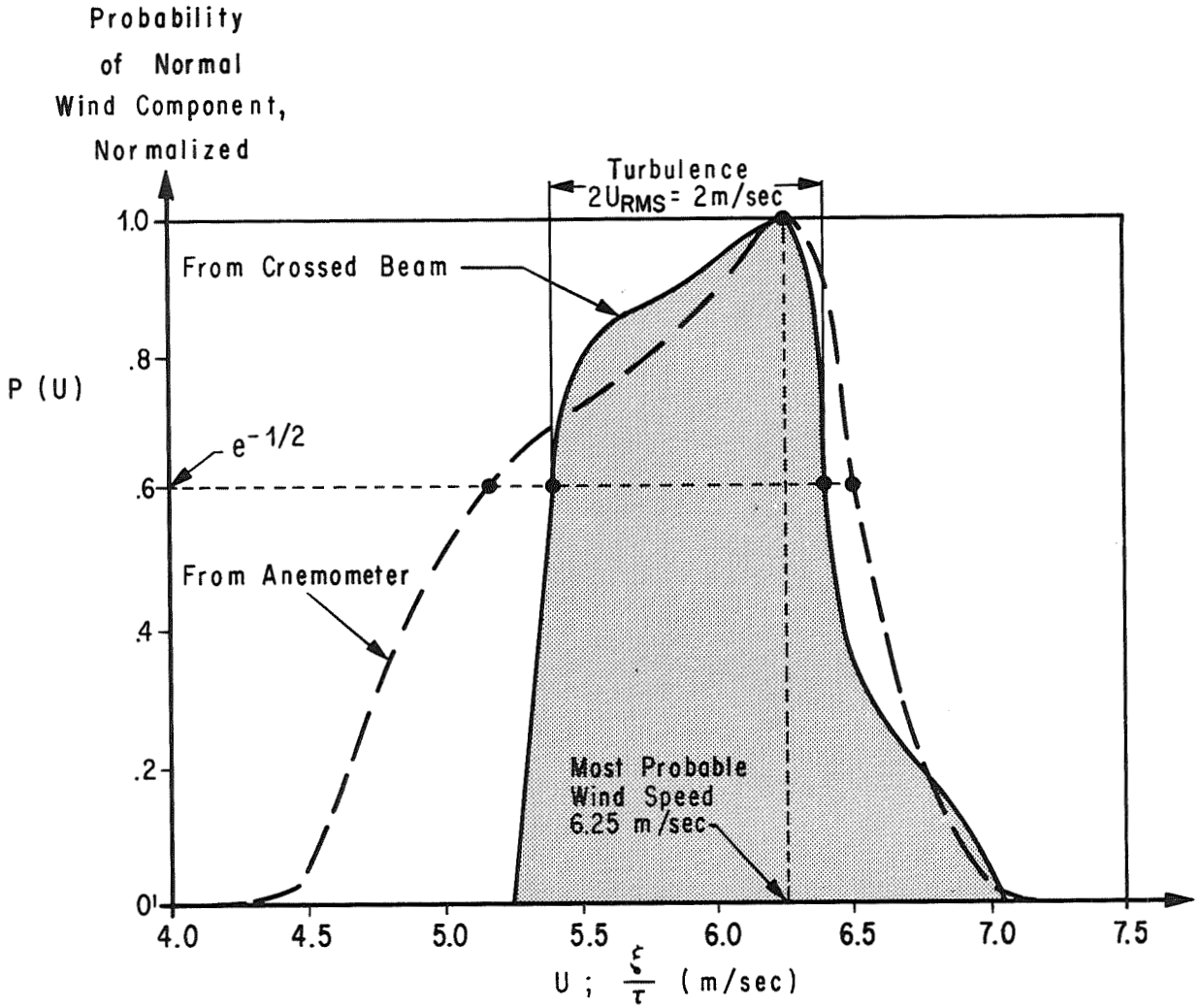

FIGURE IV.21. PROBABILITY DENSITY OF WIND COMPONENT VARIATION (RUN II)

REFERENCES

IV-1. Stephens, J. B., V. A. Sandborn, and A. J. Montgomery: Remote wind detection with the crossed-beam method at tower heights. NASA TM X-53782, October 1968.

IV-2. Sandborn, V. A. and D. J. Pickelner: Measurements of wind speeds with an optical cross-beam system. Ann. Inter. Aeroscience Electronics Symp., Washington, D. C., 1969.

IV-3. Krause, F. R., M. Y. Su, and E. H. Klugman: Passive optical detection of meteorological parameters in launch vehicle environments. To be published in Applied Optics in a special issue on Remote Sensing Techniques.

IV-4. Su, M. Y., J. B. Stephens, and M. Phillips: The theory for the determination of wind velocity and the associated altitude by the crossed-beam method. NASA TM X-53782, October 1968.

IV-5. Heybey, W. H.: The use of a ground-based multiple-beam detector in crossed-beam atmospheric experimentation. NASA TM X-53813, January 1969.

IV-6. Fisher, M. J. and F. R. Krause: The crossed-beam correlation technique. J. Fluid Mech., Vol. 28, 1967.

IV-7. Batchelor, G. K.: The Theory of Homogeneous Turbulence. The University Press, Cambridge, 1956.

IV-8. Lumley, J. L. and H. A. Panofsky: The Structure of Atmospheric Turbulence. Interscience, 1964.

IV-9. Sutton, O. G.: Micrometeorology. McGraw-Hill, 1953.

IV-10. Su, M. Y: Statistical error and required averaging time for evaluating cross-correlation of crossed-beam data. Northrop-Huntsville Tech. Memo M-794-8-362, May 1968. To be published as a NASA-CR.

IV-11. Su, M. Y.: Quantization errors and their reduction for digital time histories. To be published as a NASA Contractor Report.

IV-12. Taylor, J. T.: Digital filters for non-real time data processing. NASA CR-880, 1967.

IV-13. Graham, R. J.: Determination and analysis of numerical smoothing weights. NASA TR R-179, 1963.

IV-14. Krause, F. R., J. A. Jones and M. J. Fisher: Digital analysis of random processes by piecewise estimated covariance functions. To be published as a NASA-TR.

IV-15. Krause, F. R. and B. C. Hablutzel: Noise elimination by piecewise cross-correlation of photometer outputs. NASA TM X-53782, October 1968.

IV-16. Jayroe, R. R., Jr. and M. Y. Su: Optimum averaging times of meteorological data with time dependent means. NASA TM X-53782, October 1968.